STRING-ORDER IN MULTILEG KITAEV-HEISENBERG LADDERS

Yannick Castonguay-Page

A Thesis Submitted to the School of Graduate Studies in Partial Fulfillment of the Requirements for Master of Science

April 29, 2022

McMaster University
Master of Science (2022)
Hamilton, Ontario (Department of Physics and Astronomy)

TITLE: String-Order in multileg Kitaev-Heisenberg Ladders
AUTHOR: Yannick Castonguay-Page
SUPERVISOR: Dr. Erik S. Sørensen
NUMBER OF PAGES: 72

Acknowledgments

This thesis would not have been possible without the help of many people along the way. First and foremost, to my supervisor Erik Sørensen I say thank you for your help and patience along the way. You have taught me many things and your eye for spotting mistakes in my codes never fails to amaze me.

À Normand et à Deny, vous avez été mes premiers mentors dans le monde de la physique. Au-delà des connaissances que vous m'avez enseignées, je serais toujours reconnaissant pour les leçons et les valeurs que vous m'avez transmises. Vous êtes tous les deux de grandes inspirations pour moi. J'espère pouvoir un jour être un peu comme vous.

To John and James, thank you for your help and friendship, whether it was helping me understand an advanced statistical mechanics concept, spotting a bug in my code or simply distracting me with your conversations about the Roman Empire, I will remember the time spent in our office fondly. To Liam, thank you for being a friend during my time at McMaster. And to all the friends I've made in the Hamilton ultimate frisbee community, thank you for being amazing and welcoming.

À mes parents, votre soutien tout au long de mes études a été indispensable. Votre patience, votre écoute et votre compréhension m'ont beaucoup aidé tout au long de mon cheminement académique.

Lastly, thank you Hannah. You've been with me since the start of my journey at McMaster, through all of the ups and the downs. This Master's degree has been the most challenging thing I've ever done and you've played a big role in pushing me over the finish line. Thank you for being both a kind listener and a stern kick in the butt when I needed it.

Abstract

The Kitaev model has become a source of much excitement in the field of condensed matter. It is a two dimensional model of spins $1/2$ on a honeycomb lattice with bond-dependent interactions. Its interesting properties include a quantum spin liquid ground state and anyonic excitations. These properties could lead to exciting applications in quantum computing if materials were found to behave similarly to the Kitaev model. Such materials have been found, however the Kitaev model is too simple to describe these materials and additional interactions must be considered. The Heisenberg interaction is one such additional interaction. As such, we can define the Kitaev-Heisenberg model by combining the Kitaev and Heisenberg interactions. We can now ask ourselves if the quantum spin liquid ground state and anyonic excitations still exist in the Kitaev-Heisenberg model. To answer this question, a non-local string order parameter has been defined which is non-zero inside the quantum spin liquid phase and zero outside of it. This string order parameter was shown to exist and survive the Heisenberg interaction on the 2-leg ladder. In this thesis, we look to expand this result to multileg ladders such as the 3-leg, 4-leg, and 5-leg ladders to see if the string order parameter survives in the Kitaev-Heisenberg model in 2 dimensions. Our results show that the string order parameter does exist in multileg ladders, however the phase space window in which it survives the Heisenberg interaction is narrower than in the 2-leg ladder.

Contents

Chapter 1

Introduction

Within the field of condensed matter physics, the study of spin liquids has arisen as a hotbed of modern research. In particular, quantum spin liquids (QSL) have captured the imagination of researchers worldwide. These bizarre materials exhibit new quantum states of matter that are yet to be fully understood and could lead to new and exciting applications. Quantum spin liquids can even be difficult to define. Savary and Balents define a QSL as a system of quantum spins which are highly correlated with one another, yet do not display order even at very low temperature. Additionally, they argue that the key ingredient of a QSL is the presence of an anomalously high degree of entanglement [1].

Yet what is entanglement? While the Merriam-Webster web dictionary defines it as the state of being entangled, with entangle being a verb meaning to wrap or twist together [2], the word takes on a whole new meaning in the quantum sense. Savary and Balents define entanglement as "a property of certain quantum states, that in those states, the result of a measurement of one observable affects the outcome of the measurement of others" [1]. In quantum systems, particles exist in a superposition of states. However, when a measurement is performed, these particles are projected onto a specific state which becomes the observed state. In entangled systems, when making a measurement on one particle, this affects not only the state of the observed particle, but also the state of the entangled particles. As such, in a QSL, measuring one particle gives us information not only on that specific particle but also on the rest of the system due to the highly entangled nature of a QSL.

This high level of entanglement leads to exciting possibilities, notably in the field of quantum computing. It turns out that entanglement is a key ingredient necessary for exponential speed-up in quantum computation on pure states [3]. Ever since P. W. Shor proposed an

algorithm for factoring integers in polynomial time on quantum computers [4] thus proving their usefulness, researchers have been searching for ways to build one. Given the highly entangled nature of quantum spin liquids, they could provide the building blocks necessary for the physical realisation of a quantum computer.

However, entangled systems can be notoriously delicate. Indeed, the slightest perturbation such as thermal fluctuations or magnetic interference can ruin the entanglement. This is known as the decoherence problem [5]. One can easily imagine how difficult it would be to store information on a qubit if we can't reliably maintain said qubit in the desired state.

When searching for a way around this problem, Alexei Kitaev showed that fault-tolerant quantum computation can be achieved by exotic quasiparticles called anyons [6]. These anyons exist only in two dimensional systems and behave differently from fermions or bosons. Traditionally in quantum many-body systems, taking one particle in a loop around another particle makes the wavefunction acquire a phase $\mathrm{e}^{\mathrm{i}\theta}$ with $\theta = 0$ for bosons and $\theta = \pi$ for fermions. However, in the case of anyons, the value of θ can take any value different from 0 or π, leading to new statistics [7].

By making use of the special properties of anyons, specifically anyons obeying non-Abelian statistics, Kitaev showed that swapping anyons (known as "braiding") allows one to store quantum information in a state that is immune to local perturbations. Given this, a system with anyonic excitations is said to be in a topological phase of matter as it is robust to perturbations as long as the topology of the system is preserved. Computational operations on such a system is known as topological quantum computing. Nayak, Simon, Stern, Freedman, and Das Sarma give a more thorough review of non-Abelian anyons and their use in topological quantum computing in their article "Non-Abelian Anyons and Topological Quantum Computation" [8].

Kitaev followed up his article on fault-tolerant quantum computation with anyons by proposing an exactly solvable model which possesses anyonic excitations [9]. The model in question, now known as the Kitaev model, is a two dimensional model of spin 1/2 on a honeycomb lattice with bond-dependent interactions. Figure 1.1 shows the Kitaev lattice.

On this lattice is defined the Kitaev Hamiltonian [9] given by equation 1.1, with σ being Pauli matrices for spin 1/2 and J_i being a strength parameter :

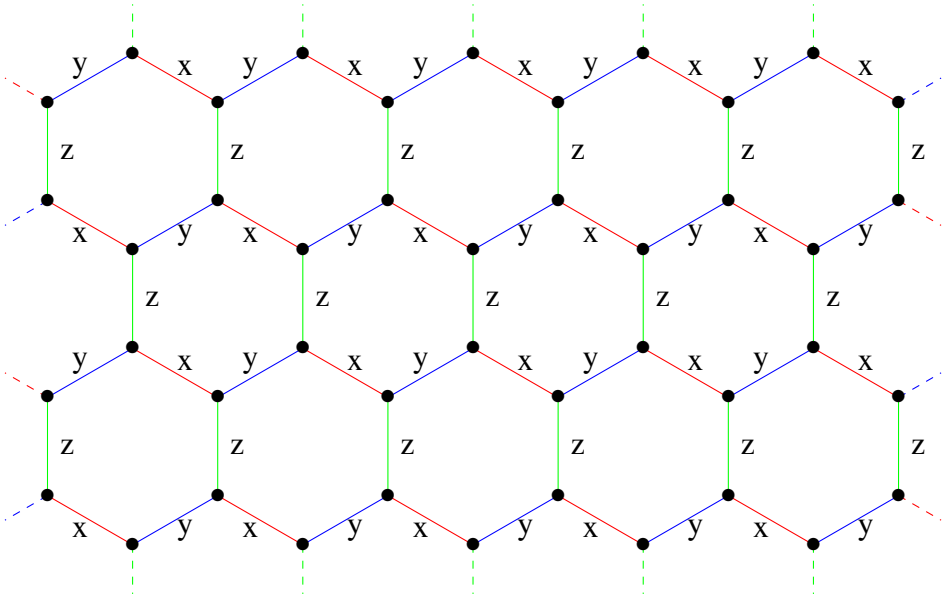

Figure 1.1: 2D Kitaev honeycomb lattice. The bond-dependent nature of the interactions is shown by the x, y, and z labels.

$$H = J_x \sum_{x-links} \sigma_j^x \sigma_k^x + J_y \sum_{y-links} \sigma_j^y \sigma_k^y + J_z \sum_{z-links} \sigma_j^z \sigma_k^z. \tag{1.1}$$

Due to the bond-dependent nature of the interactions, the model exhibits a spin liquid phase as its ground state. Normally, spin liquids arise from frustration built into the model [10]. The traditional example of frustration is geometric frustration on a triangular lattice with nearest-neighbour interactions. Due to the triangular lattice, all three spins cannot be antiparallel thus inducing fluctuations in the orientation of the three spins. Being on a honeycomb lattice, the Kitaev model does not display geometric frustration, however due to the bond-dependent nature of interactions between nearest neighbours, a chemical frustration is introduced leading to the quantum spin liquid phase.

Naturally, a material which behaves like the Kitaev model would be a great candidate for topological quantum computation. Thus following the publication of Kitaev's model, the search was on to find materials that could be described using the Kitaev model. Several candidate materials have been identified as having Kitaev-like characteristics, such as $\mathrm{Na_2IrO_3}$ [1, 11] and $\alpha\mathrm{RuCl_3}$ [1, 12]. However, the Kitaev model is too simple by itself to describe real materials. As such, additional terms must be considered in the Hamiltonian.

Chaloupka, Jackeli, and Khaliullin considered adding a Heisenberg type interaction to the Kitaev Hamiltonian when trying to describe iridium oxides [13]. Later on, Rau, Lee, and Kee showed that an additional off-diagonal term dubbed the "Γ-term" may be necessary along with the Heisenberg term to fully describe these materials [14]. For the purposes of this thesis, we will omit the Γ-term and focus our attention on the Kitaev-Heisenberg Hamiltonian.

While these additional interactions allow the model to more closely represent real materials, it comes at the cost of adding considerable complexity to the model. This new Kitaev-Heisenberg model is no longer exactly solvable and must be studied computationally. Chaloupka, Jackeli, and Khaliullin were able to study the Kitaev-Heisenberg model computationally and show the existence of a spin liquid phase, but they were limited to a cluster of only 24 sites [15]. Ideally, we want to be able to study larger systems to more accurately represent real materials.

However, the computational requirements to obtain the ground state of the model quickly become unmanageable when a large number of sites is considered. For this reason, additional modifications must be made to the model in order to make it computationally manageable while still retaining enough complexity to display the essential behaviour of the original model.

Feng, Zhang, and Xiang showed that the Kitaev model can be restricted to a 2-leg ladder geometry while still retaining most of its important properties [16]. This 2-leg ladder geometry has the advantage of being much easier to treat computationaly due to the lower number of total interactions. One of these properties is the existence of a non-local string order parameter characterising the topological quantum phase transitions present in the model.

Following this result, it becomes interesting to study the Kitaev-Heisenberg model on a 2-leg ladder. This model has the advantage of being approachable computationally while still keeping the essence of the Kitaev-Heisenberg model. Catuneanu, Sørensen, and Kee were able to show that the non-local string order parameter present in the 2-leg ladder of the Kitaev-model survives a Heisenberg interaction [17]. Thus, inside a certain window of parameters where the Heisenberg interaction is small enough, the Kitaev-Heisenberg model remains a good candidate for topological quantum computation.

Naturally, the question remains whether or not a real Kitaev material can be used for topological quantum computation. While these results are promising, it remains to be seen

whether or not a real Kitaev material described by the full Kitaev-Heisenberg model can be used as a building block for topological quantum computing. In this thesis, we attempt to bridge the gap between the results obtained on the 2-leg ladder of the Kitaev-Heisenberg model and a more complete model describing a real material by studying the Kitaev-Heisenberg model on the 4-leg ladder, the natural extension of the 2-leg ladder. We will additionally briefly define and study the 3-leg ladder and 5-leg ladder systems in an attempt to answer whether or not the non-local string order survives the Heisenberg interaction in the n-leg Kitaev-Heisenberg ladder.

This thesis is divided into a number of chapters describing the theory before going into the various results obtained. Chapter 2 of the thesis will present the Kitaev-Heisenberg model and its properties in more detail, along with the relevant modifications to the model. Chapter 3 will give a theoretical development of the string order parameter in the 2-leg ladder and its extension to the 4-leg ladder. In chapter 4 we discuss the numerical methods used to study the models. Chapter 5 discusses the various results obtained. Finally the last chapter gives the conclusions drawn from our results and suggests the next steps to follow.

Chapter 2

Kitaev-Heisenberg Ladder Models

The model of interest in this thesis is the Kitaev-Heisenberg ladder model. Before jumping straight into this model, let's first take a look at the original Kitaev model before building up to the model of interest. Once this groundwork has been established, in each subsection we will look at different modifications on the Kitaev-Heisenberg model.

2.1 Kitaev Model With Heisenberg Interaction

The original Kitaev model [9] is a two-dimensional spin 1/2 system where each spin is located at the vertices of a honeycomb lattice, as shown in figure 2.1.

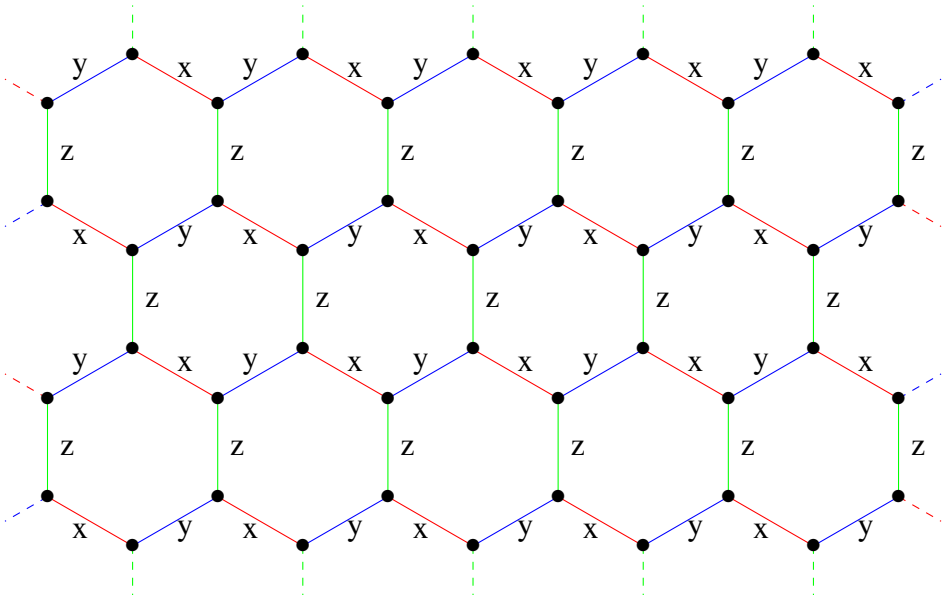

Figure 2.1: 2D honeycomb Kitaev model

As seen in this figure, each lattice site is connected by a bond-dependent interaction between nearest neighbours. Thus, three different kinds of interactions are present in the model, an x interaction (red bonds), a y interaction (blue bonds) and a z interaction (green bonds). These interactions are described by the following Hamiltonian.

$$H = J_x \sum_{x-links} \sigma_j^x \sigma_k^x + J_y \sum_{y-links} \sigma_j^y \sigma_k^y + J_z \sum_{z-links} \sigma_j^z \sigma_k^z. \tag{2.1}$$

In this Hamiltonian, σ_i^γ refers to a spin 1/2 Pauli matrix σ^γ with $\gamma \in \{x, y, z\}$ at site i of the lattice while J_γ is a strength parameter for each bond-dependent interaction. The beauty of this model is that it is exactly solvable. Not only that, but frustration is present in the model due to the bond-dependent interactions. This leads to the formation of a quantum spin liquid in the ground state with anyonic excitations.

In his article, Kitaev solves this Hamiltonian and shows the existence of 4 different phases in the ground state [9]. The phase diagram is presented in figure 2.2.

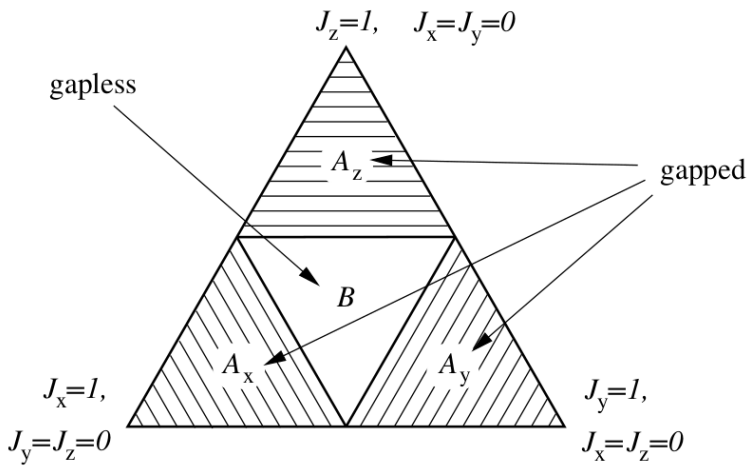

Figure 2.2: Phase diagram of the Kitaev model. Figure taken from [9].

Kitaev describes 4 different phases, A_x, A_y, A_z, and B, which are differentiated by the given values of J_x, J_y, and J_z. He also shows that the A phases are gapped while the B phase is gapless. For the purposes of this thesis, we will limit ourselves to the gapless phase by setting $J_x = J_y = J_z = K$. We introduce the variable K to parametrize the strength of the Kitaev interactions. As such, we can rewrite our isotropic Kitaev Hamiltonian in the following manner.

$$H = K \sum_{\gamma \in \langle i,j \rangle} S_i^\gamma S_j^\gamma. \tag{2.2}$$

Here γ takes the values $\gamma \in \{x, y, z\}$ for the x, y, z bonds respectively and the notation $\langle i, j \rangle$ refers to a sum over nearest neighbours. We have replaced the Pauli matrices σ with the spin operator S for spin 1/2. This operator is related to the Pauli matrices by $S = 1/2\sigma$. The factor of 2 is absorbed in the variable K.

While this model is exactly solvable, it is too simple to accurately describe real materials. Some real materials, such as α-$RuCl_3$, Na_2IrO_3, and other iridium oxides have been shown to exhibit Kitaev behaviour [1, 11–13] but are best described by adding perturbations to the model. The most common of these perturbations is a Heisenberg interaction between nearest neighbours on the honeycomb lattice. Adding a Heisenberg interaction to the Kitaev model adds a term to the Hamiltonian, which is now given as follows.

$$H = K \sum_{\gamma \in \langle i,j \rangle} S_i^\gamma S_j^\gamma + J \sum_{\langle i,j \rangle} \mathbf{S}_i \cdot \mathbf{S}_j \tag{2.3}$$

Here the variable J controls the strength of the Heisenberg perturbation. With this Heisenberg perturbation, the model is referred to as the Kitaev-Heisenberg model. Given this more realistic model, the question now becomes whether or not the interesting properties of the Kitaev model such as the spin liquid ground state and anyonic excitations survive the Heisenberg perturbation. In order to answer this question, Chaloupka, Jackeli, and Khaliullin mapped out the phase diagram of the Kitaev-Heisenberg model on a hexagonal 24-site cluster [15]. What they found was that the spin liquid phase does survive the Heisenberg interaction for a certain range of parameters. They first start from a slightly different Hamiltonian which we will label H_{CJK} given below.

$$H_{\text{CJK}} = 2K \sum_{\gamma \in \langle i,j \rangle} S_i^\gamma S_j^\gamma + J \sum_{\langle i,j \rangle} \mathbf{S}_i \cdot \mathbf{S}_j. \tag{2.4}$$

They then parametrize K and J by setting $K = A \sin\phi$ and $J = A \cos\phi$ with the energy scale $A = \sqrt{K^2 + J^2}$. By varying the angle ϕ from 0 to 2π, they are able to sweep through the whole phase space of the model. Figure 2.3 shows the phase diagram they obtained for the Kitaev-Heisenberg model on a 24-site hexagonal cluster.

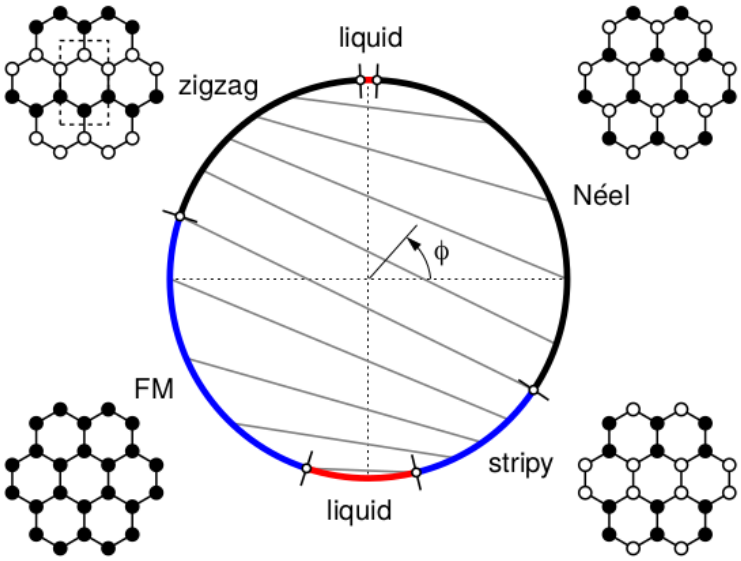

Figure 2.3: Phase diagram of the Kitaev-Heisenberg model on a 24-site hexagonal cluster. Figure taken from [15].

Of particular interest are the points where $\phi = \pi/2$ and $\phi = 3\pi/2$. At these points, we have $K = 1$ and $K = -1$ respectively and the model reduces to the exactly solvable Kitaev model. We will refer to these points as the Kitaev points, and more specifically as the anti-ferromagnetic Kitaev (AFK) point for $\phi = \pi/2$ and the ferromagnetic Kitaev (FK) point for $\phi = 3\pi/2$. Their results show that the spin liquid phase survives the Heisenberg interaction in a narrow range of parameters around the AFK point and a wider range of parameters around the FK point.

2.2 2-leg ladder

While these results are encouraging, the 24-site hexagonal cluster remains a small system and it remains unclear whether or not these results will translate to a real Kitaev material containing much more than 24 particles. When trying to include more sites, we are limited by the need to preserve the hexagonal geometry. This results in the computational resources needed quickly becoming very large due to the large number of sites and the added complexity of the Heisenberg interaction. To circumvent this problem, we can look at different lattice geometries that preserve the properties of the Kitaev model while alleviating the computational difficulties associated with a complete 2D honeycomb lattice.

One such geometry is the 2-leg ladder geometry, where we restrict the vertical axis to only two rows of sites or a single row of hexagons, but allow the horizontal axis to contain as many sites as needed. The 2-leg ladder remains identical to the full 2-D model in that it is a spin 1/2 system with both a Kitaev interaction and a Heisenberg interaction. Figure 2.4 shows the 2-leg Kitaev-Heisenberg ladder lattice.

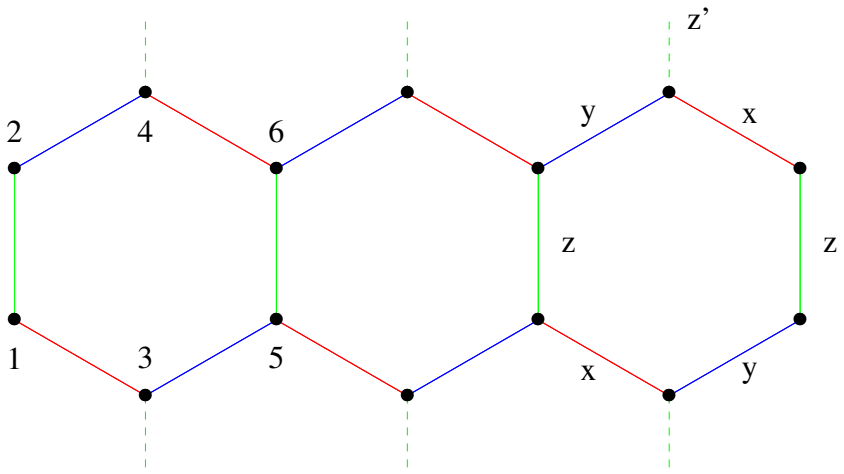

Figure 2.4: 2-leg ladder Kitaev-Heisenberg lattice

As shown in this figure, the 2-leg ladder reduces the full 2-D lattice to two rows of length L coupled by a vertical z Kitaev interaction for a total of $N = 2L$ sites. Periodic boundary conditions are used along the vertical axis indicated by the dashed lines labelled z' while open boundary conditions are used along the horizontal axis.

This ladder geometry was studied by Feng, Zhang, and Xiang for the Kitaev model without the Heisenberg interaction [16]. They were able to exactly solve the Kitaev model on the ladder geometry and show that the essence of the Kitaev model remains present even in the 2-leg ladder. Additionally, as we study ladder models with more legs, the behaviour of the model approaches the behaviour of the full 2D Kitaev honeycomb model.

Following this result, the ladder geometry seems like a good candidate for the computational study of the Kitaev-Heisenberg model. Catuneanu, Sørensen, and Kee took on this challenge by studying the Kitaev-Heisenberg model on a 2-leg ladder in order to find the phase diagram associated with this model [17]. For their work, they started with the following Kitaev-Heisenberg Hamiltonian.

$$H_{\text{2-leg}} = K \sum_{\gamma \in \langle i,j \rangle} S_i^\gamma S_j^\gamma + J \sum_{\langle i,j \rangle} \mathbf{S}_i \cdot \mathbf{S}_j. \tag{2.5}$$

This Hamiltonian is identical to equation 2.3, but it is defined on the finite 2-leg ladder system give by figure 2.4 instead of the full 2D lattice. From this Hamiltonian, they parametrize K and J by setting $K = \sin\phi$ and $J = \cos\phi$. They then proceed to sweep the phase space by varying ϕ from 0 to 2π and finding the ground state of the model at each value of ϕ. Figure 2.5 shows the phase diagram obtained for the Kitaev-Heisenberg model on a 2-leg ladder.

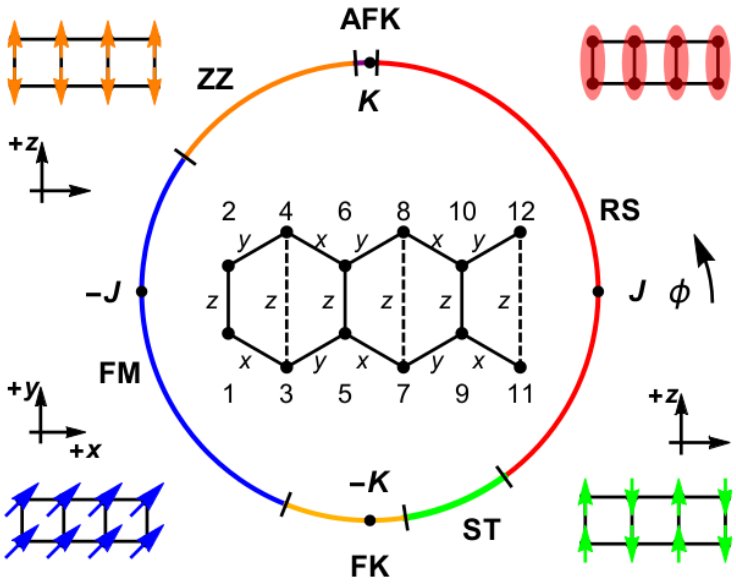

Figure 2.5: Phase diagram of the Kitaev-Heisenberg model on a 2-leg ladder. Figure taken from [17].

Much like the results obtained by Chaloupka, Jackeli, and Khaliullin [15], they found that the spin liquid phase survives the Heisenberg interaction for a certain range of parameters around the Kitaev point. However, the 2-leg ladder model has the advantage that its length can be extended significantly while still being computationally manageable, thus allowing the study of larger systems.

2.3 4-leg ladder

While the results obtained on a hexagonal cluster and on a 2-leg ladder both show that the spin liquid state survives the Heisenberg interaction around the Kitaev points, the question

remains to see whether or not these results extend to the full 2D model. This thesis attempts to bridge the gap between the 2-leg ladder Kitaev-Heisenberg model and the complete 2 dimensional Kitaev-Heisenberg model by studying larger ladder systems to see if the results change significantly when scaling up the lattice size.

The natural extension of the 2-leg ladder is the 4-leg ladder, where we add a second row of hexagons. Ideally we want to see if the results obtained for the 2-leg ladder hold for the 4-leg ladder and make predictions for how these results scale in a full size system. As we keep adding legs, we better approximate the full 2D model. The 4-leg honeycomb ladder is represented by figure 2.6.

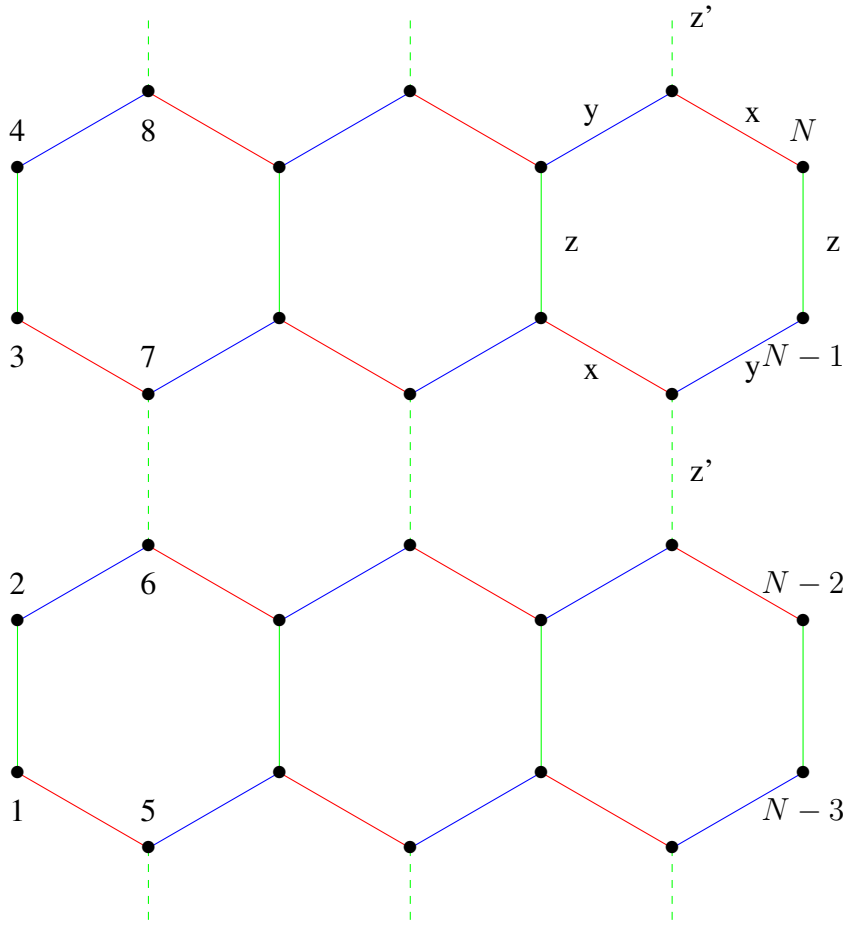

Figure 2.6: 4-leg ladder Kitaev-Heisenberg lattice

Similarly to the 2-leg ladder, we have a system composed of four rows of length L coupled by a vertical z Kitaev interaction. Periodic boundary conditions are again used along the

vertical axis while open boundary conditions are used along the horizontal axis. On this lattice we define the same Kitaev-Heisenberg Hamiltonian as for the 2-leg ladder. As such, the Hamiltonian equation remains unchanged with the exception that the sum is now on nearest neighbours of the 4-leg ladder.

$$H_{\text{4-leg}} = K \sum_{\gamma \in \langle i,j \rangle} S_i^\gamma S_j^\gamma + J \sum_{\langle i,j \rangle} \mathbf{S}_i \cdot \mathbf{S}_j \tag{2.6}$$

Of note, notice how in figures 2.4 and 2.6, the z-bonds forming the boundary conditions are labelled z'. Additionally, in figure 2.6, the z-bonds connecting both rows of hexagons are also labelled z'. If we imagine removing these bonds by setting z' to zero, the 4-leg ladder reduces to a system of two independant 2-leg ladders with open boundary conditions. We will refer to the 2-leg ladder with open boundary conditions as the "pruned" 2-leg ladder. Similarly, the 4-leg ladder where we set z' to zero will be referred to as the "pruned" 4-leg ladder.

Since the pruned 4-leg ladder is essentially two independant pruned 2-leg ladders, we expect these two pruned systems to behave the same way. Thus, by varying the strength of the z' bonds, we will be able to explore the transition between the 2-leg and 4-leg ladders and see the effect of these bonds on the behaviour of the system. By comparing the results obtained for the 2-leg pruned ladder with the results for the 4-leg pruned ladder, it will also serve as a test to confirm the validity of our results.

One of the aims of this thesis is to determine whether or not the spin liquid phase around the Kitaev points survives the Heisenberg interaction in the 4-leg ladder and if so, how the phase space around the two Kitaev points of the 4-leg ladder compares with the results obtained for the 2-leg ladder.

2.4 3-leg and 5-leg ladders

When going from the 2-leg ladder to the 4-leg ladder, an astute reader will have noticed that $\exists x \in \mathbb{N}$ such that $x \in]2, 4[$ and that number would be $x = 3$. Indeed, we have omitted to consider the 3-leg ladder, instead jumping directly to the 4-leg ladder. In this section, we take a brief look at the 3-leg and 5-leg ladder systems.

When considering a system with an odd number of legs, the vertical boundary conditions pose an additional difficulty as simply looping around to connect sites from the top leg to the

bottom leg does not preserve the hexagonal shape of the lattice. For this reason, the 4-leg ladder is a more natural extension of the 2-leg ladder compared to ladders with an odd number of legs. Nevertheless, we will attempt to study the 3-leg and 5-leg ladder systems to see if the results obtained differ substantially.

As a solution to this boundary condition conundrum, instead of connecting sites directly aligned with each other vertically, we instead *shift* the bond so a site in the top leg connects not to the corresponding site on the bottom leg, but to the site directly to the right of of the corresponding site on the bottom leg. Figure 2.7 shows the 3-leg ladder with the shifted periodic boundary conditions.

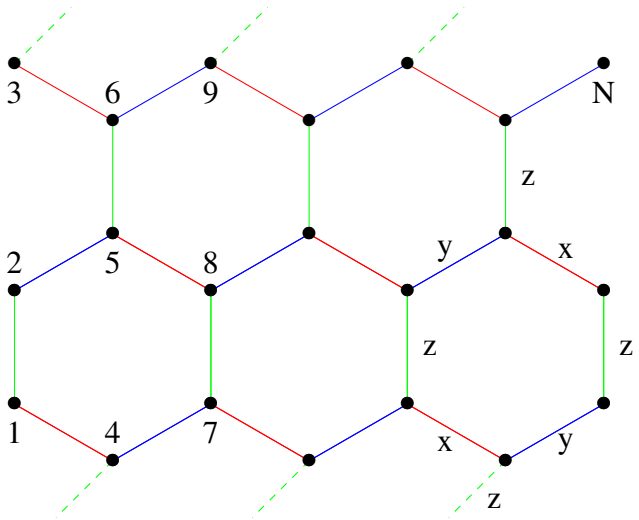

Figure 2.7: 3-leg ladder Kitaev-Heisenberg lattice

As we can see in the figure, the boundary condition at site 3 connects sites 3 and 4 together with a z interaction instead of connecting sites 3 and 1 as would be the case in an even leg ladder. More generally, the boundary conditions in the 3-leg ladder connect site n with site $n+1$ where $n = 6m+3$, $m \in \mathbb{N}$. With these shifted boundary conditions, the model becomes more akin to a spiral than a cylinder. For this reason, the results obtained may differ significantly when compared to the even leg ladders. Nevertheless, we will briefly study this 3-leg model to see if a spin liquid ground state exists around the Kitaev points. The expression of the Hamiltonian for the 3-leg ladder thus remains unchanged from the Hamiltonian for the 2-leg and 4-leg ladders, the lattice being the only difference between these models.

Similarly to the 3-leg ladder, we can consider a 5-leg ladder system. Once again, due to the odd number of legs, we cannot preserve the hexagonal shape with traditional boundary

conditions and must instead use shifted boundary conditions. Figure 2.8 shows the lattice used for the 5-leg ladder Kitaev-Heisenberg model.

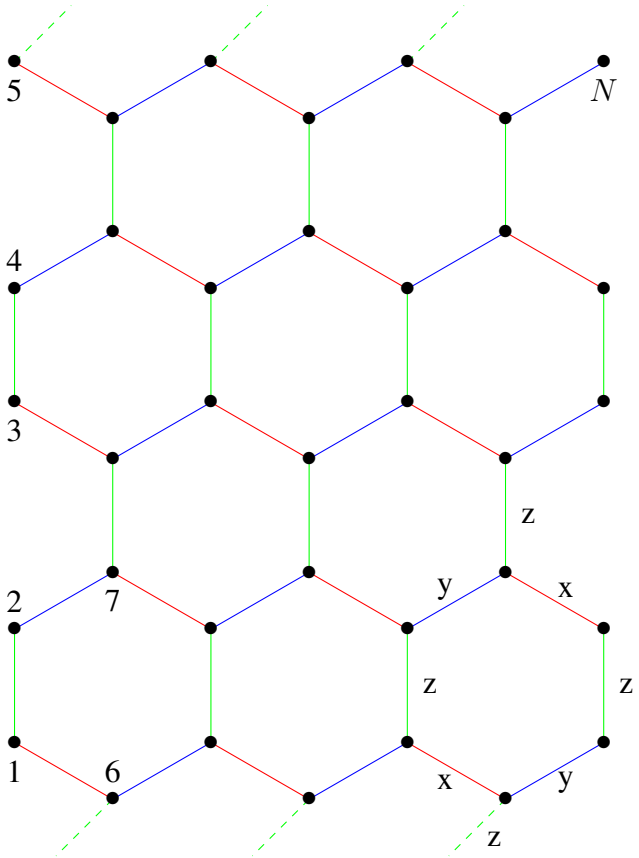

Figure 2.8: 5-leg ladder Kitaev-Heisenberg lattice

Similarly to the 3-leg ladder, the boundary conditions connect site n with site $n+1$ where $n = 10m + 5$, $m \in \mathbb{N}$. On this lattice exists the same Kitaev-Heisenberg Hamiltonian as for the even leg lattices. Once again we aim to show whether or not a spin liquid phase which survives the Heisenberg interaction exists around the Kitaev points.

We could similarly keep going and study n-leg ladder systems with n being larger than 5, but for the purposes of this thesis and due to the limitations of the computational resources available, we limit our study to ladders of 5 legs or less.

Chapter 3

String Order Parameter

Once these models have been defined by setting a lattice and a corresponding Kitaev-Heisenberg Hamiltonian, we must be able to do calculations on these models to uncover their desirable properties. We start by finding the ground state and corresponding ground state energy of the model. The exact procedure by which we find the ground state will be explained in chapter 4. In this chapter, we will go over how to identify the various phases of the ground state and the associated non-local string order parameter.

In the previous chapter, we have described various Kitaev-Heisenberg models and their corresponding phase diagrams. The different phases of these models are divided by second order phase transitions which can be described by the Landau theory of phase transitions. Normally, with each transition is associated a local order parameter. However, in disordered systems such as the spin liquid ground state of the Kitaev model, there exists no local order by definition and as such, no local order parameter can be defined. Nevertheless, a phase transition still occurs in the Kitaev-Heisenberg model when the Heisenberg interaction becomes important.

In quantum systems, a quantum phase transition can occur without an obvious associated local order parameter. Instead of a local order parameter, a non-local order parameter can be used to describe these phase transitions. Such a non-local order parameter was first described in the Kitaev ladder model by Feng, Zhang, and Xiang [16]. They found that the phase transitions of the Kitaev model at zero temperature are topological and can be characterised by non-local string order parameters. Building upon this result, Catuneanu, Sørensen, and Kee [17] showed that a non-local string order parameter exists in the Kitaev-Heisenberg model on the 2-leg ladder and the associated phase survives a Heisenberg perturbation.

In this section, we explain the procedure used by Catuneanu, Sørensen, and Kee to define and calculate the non-local string order parameter on the 2-leg Kitaev-Heisenberg ladder and how to extend this procedure to the 4-leg ladder. Much of the theory covered in this chapter was developed by Catuneanu, Sørensen, and Kee [17, 18].

3.1 Transformation of the 2-leg ladder Hamiltonian

As the ground state of the Kitaev model is a disordered spin liquid, there exists no local order parameter in the ground state of the Kitaev model. However, Catuneanu, Sørensen, and Kee were able to show the existence of a hidden long range order in the $S = 1/2$ 2-leg ladder model through a non-local string order parameter [17]. In order to do so, they consider a non-local unitary operator V acting on the 2-leg Kitaev ladder defined by equation 2.5. For this theoretical consideration, we consider only the Kitaev interaction, setting $J = 0$. The Heisenberg interaction will be considered at a later point. The non-local operator V is defined as :

$$V = \prod_{\substack{j+1<k \\ j \text{ odd}, k \text{ odd} \\ j=1,\ldots,N-3 \\ k=3,\ldots,N-1}} U(j,k). \tag{3.1}$$

In this equation, each individual $U(j,k)$ is given by :

$$U(j,k) = \mathrm{e}^{\mathrm{i}\pi\left(S^y_j + S^y_{j+1}\right)\cdot\left(S^x_k + S^x_{k+1}\right)}. \tag{3.2}$$

We see here that each $U(j,k)$ is unitary. As such, V is also unitary. The indices j, $j+1$ and k, $k+1$ form a rung of the $S = 1/2$ ladder. One property of the $U(j,k)$ operators is that they commute :

$$[U(j,k), U(l,m)] = 0 \ \forall j,k,l,m \tag{3.3}$$

which allows us to rearrange terms easily. When applying the transformation V to individual spin operators S^α_i, we find the following relations.

$$V^\dagger S^x_i V = S^x_i \prod_{\substack{j>i \\ j \text{ odd}}} \mathrm{e}^{i\pi\left(S^x_j + S^x_{j+1}\right)} \tag{3.4}$$

$$V^\dagger S_i^y V = \prod_{\substack{j<i-1 \\ j \text{ odd}}} \mathrm{e}^{i\pi\left(S_j^y + S_{j+1}^y\right)} S_i^y \tag{3.5}$$

$$V^\dagger S_i^z V = \prod_{\substack{j<i-1 \\ j \text{ odd}}} \mathrm{e}^{i\pi\left(S_j^y + S_{j+1}^y\right)} S_i^z \prod_{\substack{j>i \\ j \text{ odd}}} \mathrm{e}^{i\pi\left(S_j^x + S_{j+1}^x\right)} \tag{3.6}$$

With these relations and the fact that the spin operators relate to the Pauli matrices by $S_i^\alpha = 1/2\sigma_i^\alpha$ (here $\hbar$ is set to 1), we can now look at how the 2-leg Kitaev ladder Hamiltonian transforms under the unitary transformation V.

Starting with only a single plaquette, let's look at how the $S_1^x S_3^x$ Kitaev term is transformed by V. First, using equation 3.4, the spin operators S_1^x and S_3^x are transformed in the following way.

$$\begin{aligned} V^\dagger S_1^x V &= S_1^x \prod\nolimits_{j \text{ odd}}^{j>1} \mathrm{e}^{i\pi\left(S_j^x + S_{j+1}^x\right)} \\ &= S_1^x e^{i\pi\left(S_3^x + S_4^x\right)} \end{aligned} \tag{3.7}$$

$$\begin{aligned} V^\dagger S_3^x V &= S_3^x \prod\nolimits_{j \text{ odd}}^{j>3} \mathrm{e}^{i\pi\left(S_j^x + S_{j+1}^x\right)} \\ &= S_3^x \end{aligned} \tag{3.8}$$

Using these results, the $S_1^x S_3^x$ term in the Hamiltonian will be transformed in the following way.

$$\begin{aligned} V^\dagger S_1^x S_3^x V &= S_1^x e^{i\pi\left(S_3^x + S_4^x\right)} S_3^x \\ &= S_1^x e^{i\pi S_3^x} e^{i\pi S_4^x} S_3^x \\ &= S_1^x e^{i\frac{\pi}{2}\sigma_3^x} e^{i\frac{\pi}{2}\sigma_4^x} S_3^x \end{aligned} \tag{3.9}$$

From the properties of the Pauli matrices, we know that the exponential of a Pauli matrix can be written as :

$$e^{ia\sigma} = I\cos a + i\sigma \sin a \tag{3.10}$$

where I is the identity matrix. Using this property along with the fact that in our case $a = \pi/2$, the cosine term disappears and we are left with

$$\begin{aligned} V^\dagger S_1^x S_3^x V &= S_1^x \left(i\sigma_3^x\right)\left(i\sigma_4^x\right) S_3^x \\ &= -S_1^x \sigma_3^x (1/2\sigma_3^x)\sigma_4^x \\ &= -S_1^x S_4^x \end{aligned} \tag{3.11}$$

where we have used the property that Pauli matrices square to the identity. Similarly, the same process for the $S_2^y S_4^y$ term yields the following result :

$$V^\dagger S_2^y S_4^y V = -S_1^y S_4^y. \tag{3.12}$$

For the last two interaction terms on the plaquette, we find that $S_1^z S_2^z$ and $S_3^z S_4^z$ remain unchanged by V. The same analysis on a plaquette where the x and y interactions are flipped yields a similar result, namely $V^\dagger S_2^x S_4^x V = -S_2^x S_3^x$ and $V^\dagger S_1^y S_3^y V = -S_2^y S_3^y$. Given this, the unitary operator V has the effect of moving the x and y bonds and changing the sign of the interaction. This transformation is sketched in figure 3.1.

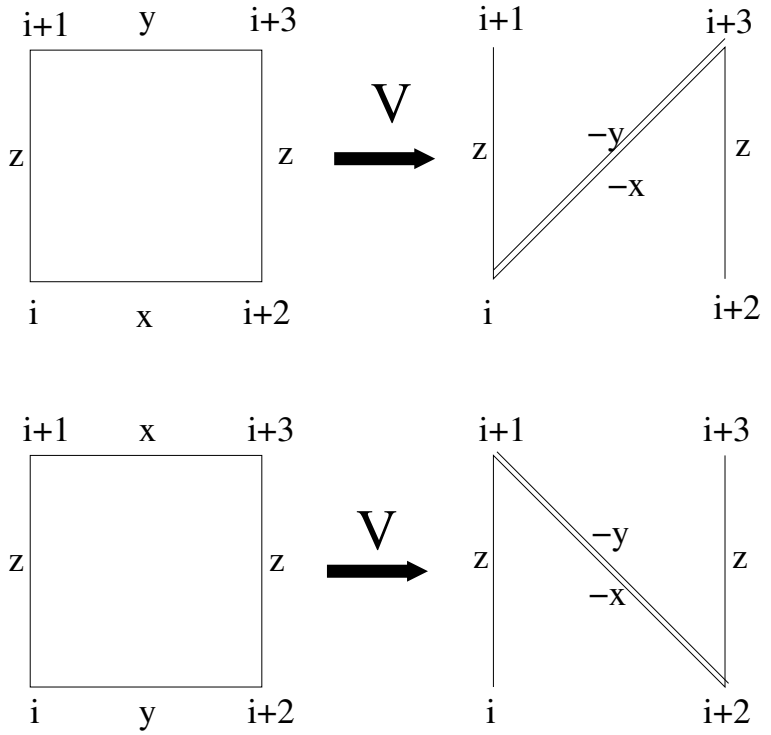

Figure 3.1: Transformation of a plaquette by the unitary operator V. Figure taken from [18].

These transformations also apply not only to the first plaquette, but to all other plaquettes. Thus, when applying the unitary operator V to the full 2-leg ladder Kitaev Hamiltonian, it is transformed into a "dangling-Z" model represented in the figure below.

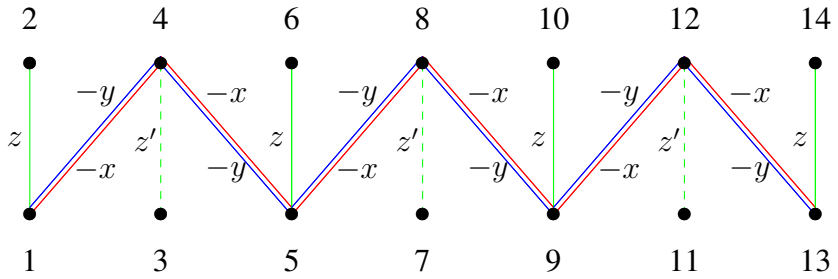

Figure 3.2: Transformed "dangling-Z" Hamiltonian

Given the nature of this transformation, open boundary conditions along the horizontal axis are paramount to the success of this method. The corresponding Hamiltonian with this transformed model is given by $V^\dagger H V = H_{d-Z}$ with [17] :

$$H_{d-Z} = K \sum_{n=0} \tilde{S}^z_{2n+1} \tilde{S}^z_{2n+2} - K \sum_{n,\alpha=x,y} \left(\tilde{S}^\alpha_{4n+1} \tilde{S}^\alpha_{4n+4} + \tilde{S}^\alpha_{4n+4} \tilde{S}^\alpha_{4n+5} \right) \tag{3.13}$$

where $\tilde{S}$ denotes spins in H_{d-Z}. At the Kitaev points, this transformed Hamiltonian is simply an XY chain with an Ising coupling to a dangling spin at every site. It is clear then that there is long range order on this transformed Hamiltonian. In the presence of a non-zero Heisenberg term, the transformed Hamiltonian becomes more complicated, but it remains to be seen if this long range-order persists through the Heisenberg perturbation.

3.2 String order parameter in the 2-leg ladder

Seeing that H_{d-Z} can have long-range order in the sense that $\lim_{r\to\infty} \left\langle \tilde{S}^\alpha_i \tilde{S}^\alpha_{i+r} \right\rangle \neq 0, \alpha = x, y, z$, we can define an ordinary correlation function in the transformed Hamiltonian H_{d-Z} that corresponds to a string correlation function in the original Hamiltonian H. Starting from the first dangling spin at site 2, let's have a look at the correlation function $\left\langle \tilde{S}^z_2 \tilde{S}^z_{2+r} \right\rangle$. For $r = 1$, we have :

$$\left\langle \tilde{S}^z_2 \tilde{S}^z_3 \right\rangle = V^\dagger S^z_2 S^z_3 V \tag{3.14}$$

Using equation 3.6 and a similar process as when we transformed the Hamiltonian, we find the following results on a single plaquette :

$$V^\dagger S^z_2 V = -\frac{1}{2} \sigma^z_2 \sigma^x_3 \sigma^x_4 \tag{3.15}$$

$$V^{\dagger} S_3^z V = -\frac{1}{2}\sigma_1^y \sigma_2^y \sigma_3^z \tag{3.16}$$

Using these results to solve equation 3.14, we find :

$$\begin{aligned} \left\langle \tilde{S}_2^z \tilde{S}_3^z \right\rangle &= \left(-\frac{1}{2}\right)^2 \sigma_1^y \sigma_2^z \sigma_2^y \sigma_3^x \sigma_3^z \sigma_4^x \\ &= \frac{1}{4}\sigma_1^y \left(-i\sigma_2^x\right)\left(-i\sigma_3^y\right)\sigma_4^x \\ &= -\frac{1}{4}\sigma_1^y \sigma_2^x \sigma_3^y \sigma_4^x \end{aligned} \tag{3.17}$$

where we have made use of the Pauli matrix property that $\sigma_j \sigma_k = i\epsilon_{jkl}\sigma_l$ with ϵ_{jkl} being the Levi-Civita symbol and $j \neq k$. From this result, we define the string order parameter $\langle O^z(r) \rangle$ in the following way :

$$\langle O^z(r) \rangle = 4 \left\langle \tilde{S}_2^z \tilde{S}_{2+r}^z \right\rangle \tag{3.18}$$

As such, by going through the same process to determine the other values of the string order parameter, we find :

$$\begin{aligned} \langle O^z(1) \rangle &= 4 \left\langle \tilde{S}_2^z \tilde{S}_3^z \right\rangle = -\sigma_1^y \sigma_2^x \sigma_3^y \sigma_4^x \\ \langle O^z(2) \rangle &= 4 \left\langle \tilde{S}_2^z \tilde{S}_4^z \right\rangle = -\sigma_1^y \sigma_2^x \sigma_3^x \sigma_4^y \\ \langle O^z(3) \rangle &= 4 \left\langle \tilde{S}_2^z \tilde{S}_5^z \right\rangle = \sigma_1^y \sigma_2^x \sigma_3^z \sigma_4^z \sigma_5^y \sigma_6^x \\ \langle O^z(4) \rangle &= 4 \left\langle \tilde{S}_2^z \tilde{S}_6^z \right\rangle = \sigma_1^y \sigma_2^x \sigma_3^z \sigma_4^z \sigma_5^x \sigma_6^y \\ \langle O^z(5) \rangle &= 4 \left\langle \tilde{S}_2^z \tilde{S}_7^z \right\rangle = \sigma_1^y \sigma_2^x \sigma_3^z \sigma_4^z \sigma_5^z \sigma_6^z \sigma_7^y \sigma_8^x \\ \langle O^z(6) \rangle &= 4 \left\langle \tilde{S}_2^z \tilde{S}_8^z \right\rangle = \sigma_1^y \sigma_2^x \sigma_3^z \sigma_4^z \sigma_5^z \sigma_6^z \sigma_7^x \sigma_8^y \end{aligned} \tag{3.19}$$

Generalising these results, we find that the string order parameter as defined by equation 3.18 on the 2-leg ladder is given by the following equation :

$$\begin{aligned} \langle O^z(r) \rangle_{2-leg} &= (-1)^{\lfloor (r+1)/2 \rfloor} \\ &\times \begin{cases} \langle \sigma_1^y \sigma_2^x (\prod_{k=3}^{r+1} \sigma_k^z) \sigma_{r+2}^y \sigma_{r+3}^x \rangle & r \text{ odd} \\ \langle \sigma_1^y \sigma_2^x (\prod_{k=3}^{r} \sigma_k^z) \sigma_{r+1}^x \sigma_{r+2}^y \rangle & r \text{ even} \end{cases} . \end{aligned} \tag{3.20}$$

Equation 3.20 gives us the equation for the string order parameter in the 2-leg ladder. From equation 3.18, we see that this non-local string order parameter is associated with a local order parameter on the transformed lattice. For this reason, conventional Landau theory

of phase transitions can be applied on the transformed lattice. On the original 2-leg lattice, this local order parameter becomes a non-local string order parameter due to the non-local nature of the transformation operator V.

At the Kitaev points, $\langle O^z(r)\rangle_{2-leg}$ is exactly 1 thus showing the existence of a hidden long range order in the Kitaev model. However, when adding the Heisenberg term, it becomes unclear if the long range order survives the extra interaction. As such, we will attempt to measure the string order parameter given by equation 3.20 on ground states of the Kitaev-Heisenberg 2-leg model around the Kitaev points to see if it remains non-zero and if so, in what range of parameters.

3.3 String order parameter in the 4-leg ladder

In this section, we look to extend the string order parameter result for the 2-leg ladder to the 4-leg ladder. Catuneanu, Sorensen, and Kee [17] showed that the string order parameter survives the Heisenberg interaction in a certain range of parameters around the Kitaev points on the 2-leg ladder. However, the 2-leg ladder remains a small system compared to potential real Kitaev materials. To remedy this problem, we now wish to turn our attention to the 4-leg ladder to see if a hidden long range order remains present in the Kitaev-Heisenberg model as we approach a full 2D model.

In order to obtain results on the 4-leg ladder that can be directly compared to the results for the 2-leg ladder, we again use equation 3.20 to calculate the string order parameter. However, given the different numbering pattern of the 4-leg ladder, we must adapt the SOP equation to match the correct sites on the 4-leg ladder. Trying to adapt equation 3.20 to match the appropriate sites on the 4-leg ladder leads to a complicated expression that becomes difficult to read and understand. Instead, we proceed by first finding a ground state of the 4-leg Kitaev-Heisenberg ladder. Once this ground state is found, we change the numbering pattern on the 4-leg ladder. Figure 3.3 shows the numbering pattern used to calculate the SOP on the 4-leg ladder.

With this numbering pattern, we can directly use equation 3.20 for calculating the string order parameter on the 4-leg ladder. As shown in figure 3.3, we number the sites on the lower half of the lattice from 1 to $N/2$, thus matching the numbering of sites in the 2-leg ladder. The additional row of hexagons in the 4-leg ladder can be considered as an additional pertur-

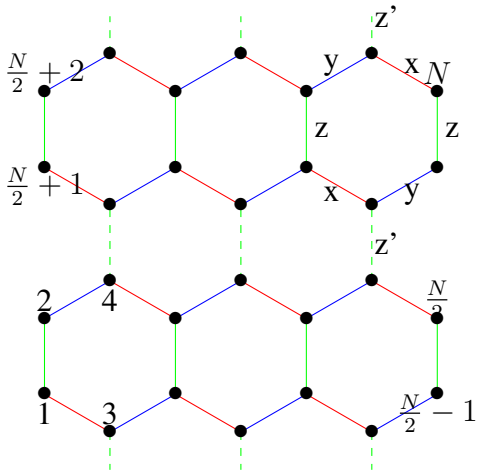

Figure 3.3: Alternative numbering on the 4-leg Kitaev-Heisenberg ladder for calculating the string order parameter

bation to the 2-leg ladder in much the same way as the Heisenberg interaction. Thus, we can ask ourselves if the string order parameter as defined by equation 3.20 survives the additional interactions present in the 4-leg ladder.

When calculating the string order parameter on the 4-leg ladder in order to compare the results with the 2-leg ladder results, it is important to make note of the interactions labelled z'. As mentioned in chapter 2, setting $z' = 0$ reduces the 4-leg ladder to two independant pruned 2-leg ladders. As such, comparing results obtained on the 4-leg pruned lattice with results of the 2-leg pruned lattice should give identical results when calculating the SOP and doing this allows us to convince ourselves of the results obtained for the 4-leg ladder.

The string order parameter in the 3 and 5 leg ladders is calculated in much the same way as with the 4-leg ladder. Once again, after finding the ground state of the system, we renumber the lattice so that the numbering of the bottom two legs matches exactly the numbering in the 2-leg ladder. Thus, by renumbering the sites, we can use equation 3.20 directly to calculate the string order parameter not only for the 2-leg ladder, but for all multileg ladder systems.

Chapter 4

Numerical Methods

Here we present the numerical methods used in this thesis to obtain our results. We have so far talked about the Kitaev-Heisenberg model on various ladders and discussed the phase space of this model while glancing over the process by which we identify the phase transitions. Additionally, we've mentionned finding the ground state of the model computationally without going into details. In this section, we will discuss the techniques used to obtain the ground state of a system starting from a set lattice with a corresponding Hamiltonian.

4.1 Density Matrix Renormalisation Group

The technique used in this thesis to find the ground state associated with a given Hamiltonian defined on a specific lattice is known as density matrix renormalization group. DMRG was first introduced by Steven R. White in 1992 [19] as a method for diagonalizing the Hamiltonian of $S = 1/2$ and $S = 1$ Heisenberg chains. It has since proven to be a very successful technique for finding ground states of almost any one-dimensional quantum lattice systems, as well as some two dimensional systems such as ladder models.

As with any problem concerning a Hamiltonian, the first goal is to find the ground state of the system. This means finding solutions to the following equation.

$$\hat{H} \left|\psi\right\rangle = E \left|\psi\right\rangle \tag{4.1}$$

Thus, this is equivalent to finding the eigenvalues and eigenstates of the Hamiltonian operator. The ground state is the eigenstate which corresponds to the smallest energy eigenvalue E. Rearranging the terms to isolate the energy, we have the following equation.

$$E = \frac{\langle\psi|\,\hat{H}\,|\psi\rangle}{\langle\psi|\psi\rangle} \tag{4.2}$$

DMRG tackles the problem of finding the ground state $|\psi\rangle$ and corresponding ground state energy E variationally by performing operations on an initial state $|\psi_0\rangle$ in order to minimise the energy E. An in depth description of the DMRG method for solving Hamiltonians can be found given by Schollwock [20].

4.2 DMRG on matrix product states

The key problem with finding the ground state of a spin $1/2$ system such as the Kitaev-Heisenberg model is that the Hilbert space born from the eigenstates of $\hat{H}$ grows as 2^N with N being the system size. DMRG circumvents this problem by considering only states of up to m dimensions with m being much smaller than 2^N the dimension of the Hilbert space. We refer to m as the bond dimension. By restricting the search for the ground state to a subspace of dimension m, the task of finding the ground state becomes much more manageable.

In order to find a good approximation to the ground state, it is important to make an informed choice of the m basis vectors which span the search space. DMRG achieves this choice of basis by first encoding the wave function as a matrix product state (MPS). A matrix product state refers to a quantum state $|\psi\rangle$expressed as a product of matrices in the following manner :

$$|\psi\rangle = \sum_{\{\sigma_i\}} A^{\sigma_1}...A^{\sigma_N}\,|\sigma_1,...,\sigma_N\rangle\,. \tag{4.3}$$

Here $|\sigma_1,...,\sigma_N\rangle$ refers to the basis states such as the Pauli matrices for $S = 1/2$ while A are matrices. Such an MPS is subject to singular value decomposition. The SVD of a matrix M is the factorization $M = UDV^\dagger$ where U and V are unitary while D is diagonal. The diagonal entries of D are referred to as the singular values of M. However, these singular values can be used as a method for approximating M. We can define a matrix $\tilde{D}$ by keeping only the m largest singular values and replacing the remaining singular values by 0. By calculating the product $\tilde{M} = U\tilde{D}V^\dagger$, we obtain a matrix $\tilde{M}$ which is a very good approximation of M.

This SVD procedure is the core element to identifying the m most relevant basis vectors for the ground state. It allows us to truncate the least relevant basis states and only consider a subspace of dimension m of the Hilbert space while still providing a good approximation of the ground state. After identifying this smaller subspace, the DMRG algorithm employs a variational procedure to find the state $|\psi\rangle$ within this subspace which minimises the energy E given by equation 4.2 by optimising the parameters of the A matrices. This state $|\psi\rangle$ then becomes a good approximation of the ground state of the system expressed as an MPS.

A much more complete description of how DMRG functions and makes use of matrix product states can be found given by Schollwock [21]

4.3 Mapping the ladder models to a 1D Hamiltonian

As DMRG was developed to solve 1 dimensional Hamiltonians, in order to use DMRG to find the ground state of the Kitaev-Heisenberg model on the 2-leg ladder, it is first necessary to convert the 2-leg ladder to a one dimensional system. To do this, we first number the sites on the 2-leg ladder from 1 to N with $N = 2L$, L being the length of the system. We then line up each site along a one dimensional chain from 1 to N. We then connect the sites to each other with the same interactions present in the 2-leg ladder. Figure 4.1 shows how each interaction in the 2-leg ladder is mapped to a one dimensional chain.

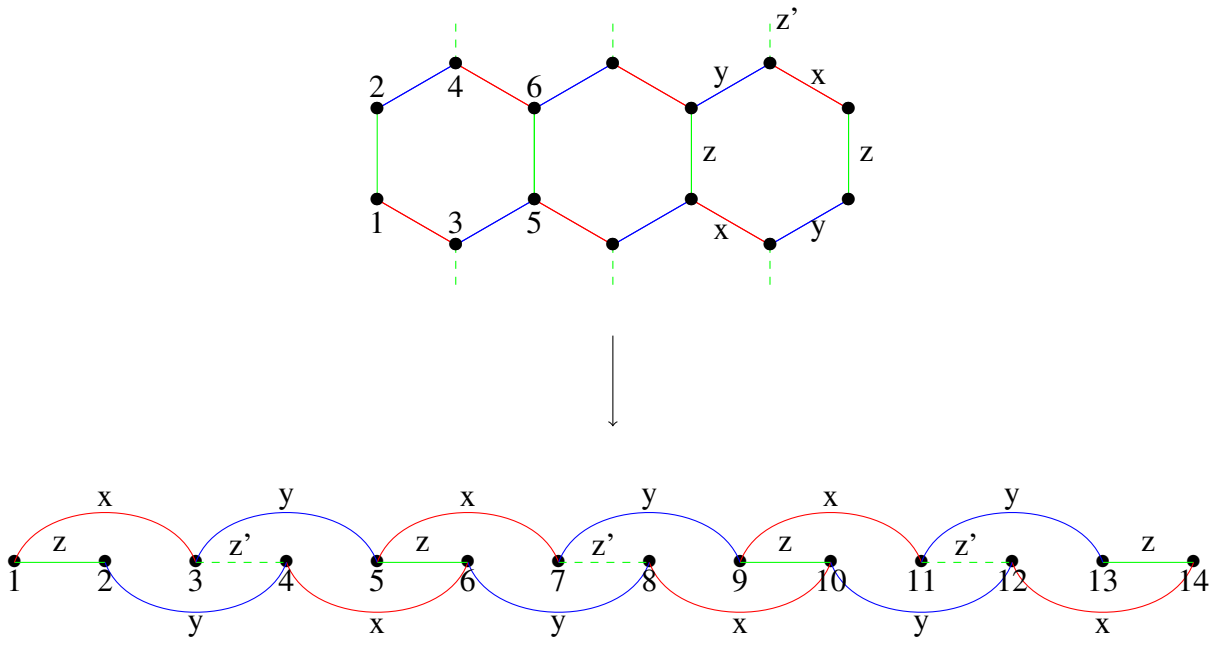

Figure 4.1: Mapping of the 2-leg ladder Kitaev-Heisenberg lattice onto a 1D chain.

We see from figure 4.1 that the 2-leg ladder maps to a 1 dimensional chain with next-nearest neighbour interactions. We can then rewrite our Kitaev-Heisenberg Hamiltonian as a one dimensional Hamiltonian based on the interactions in figure 4.1. The following equation gives the Hamiltonian for the 2-leg Kitaev-Heisenberg ladder in one dimensional form, which we label $\mathcal{H}_2$.

$$\begin{aligned}\mathcal{H}_2 = K \sum_{\substack{i=4k+1 \\ k\in\mathbb{N}}}^{N} & S_i^z S_{i+1}^z + S_i^x S_{i+2}^x + S_{i+2}^y S_{i+4}^y + S_{i+1}^y S_{i+3}^y + S_{i+3}^x S_{i+5}^x \\ + J \sum_{\substack{i=4k+1 \\ k\in\mathbb{N}}}^{N} & \mathbf{S}_i \cdot \mathbf{S}_{i+1} + J \sum_{i=1}^{N-2} \mathbf{S}_i \cdot \mathbf{S}_{i+2} \\ + \alpha \sum_{\substack{i=4k+1 \\ k\in\mathbb{N}}}^{N} & K S_{i+2}^z S_{i+3}^z + J \mathbf{S}_{i+2} \cdot \mathbf{S}_{i+3}\end{aligned} \tag{4.4}$$

Here we have defined K' and J' as $K' = \alpha K$ and $J' = \alpha J$ with α being a strength parameter for the primed interactions. Setting $\alpha = 1$ gives us the normal Kitaev-Heisenberg Hamiltonian with vertical periodic boundary conditions while setting $\alpha = 0$ reduces the Hamiltonian to the pruned model. This one dimensional Hamiltonian can then be fed into the DMRG algorithm to find the ground state of the 2-leg ladder Kitaev-Heisenberg model.

We can repeat this procedure for the 4-leg Kitaev-Heisenberg ladder and map the 4-leg Hamiltonian onto a one dimensional chain. Figure 4.2 shows how the 4-leg ladder with Kitaev-Heisenberg interactions is mapped to a one dimensional model.

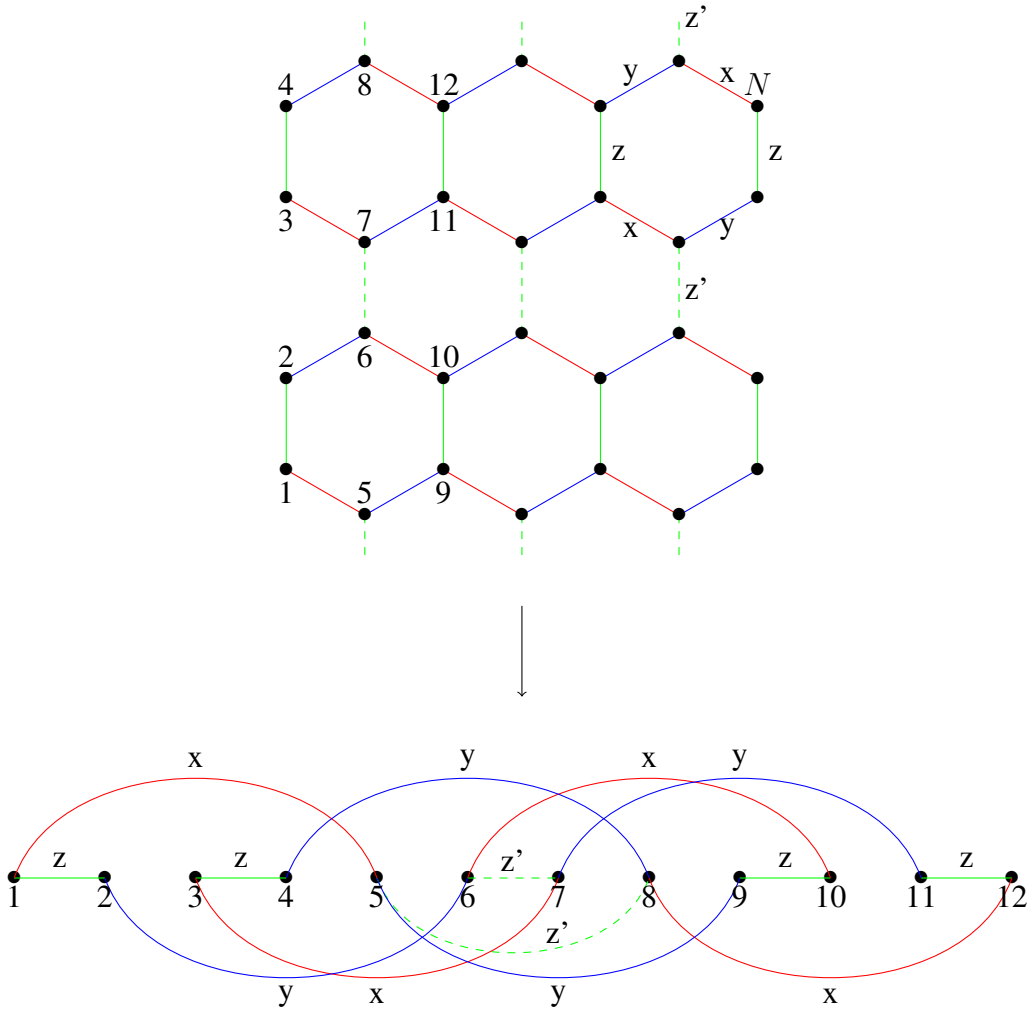

Figure 4.2: Mapping of the 4-leg ladder Kitaev-Heisenberg lattice onto a 1D chain

Here we see a similar picture as in the 2-leg ladder case, but instead of having next-nearest neighbour interactions, in the case of the 4-leg ladder we have interactions between sites situated up to 4 sites away. It is interesting to note that looking at the dashed lines labelled z', we can see that if we remove these interactions, the system becomes two independent chains who are intertwined, but do not interact with each other. Comparing these chains to the one dimensional picture of the 2-leg ladder in figure 4.1, we see that each independent chain is equivalent to a 2-leg ladder. For this reason, the pruned 4-leg ladder and the pruned 2-leg ladder should behave identically.

As we did for the 2-leg ladder, we can rewrite the 4-leg Kitaev-Heisenberg Hamiltonian as a one dimensional Hamiltonian based on the interactions shown in figure 4.2. The following

equation gives the Hamiltonian for the 4-leg ladder on a one dimensional chain.

$$\begin{aligned}\mathcal{H}_4 = K \sum_{\substack{i=8k+1 \\ k\in\mathbb{N}}}^{N} & S_i^z S_{i+1}^z + S_{i+2}^z S_{i+3}^z + S_i^x S_{i+4}^x + S_{i+4}^y S_{i+8}^y + S_{i+1}^y S_{i+5}^y + S_{i+5}^x S_{i+9}^x \\ & + S_{i+2}^x S_{i+6}^x + S_{i+6}^y S_{i+10}^y + S_{i+3}^y S_{i+7}^y + S_{i+7}^x S_{i+11}^x \\ & + J \sum_{\substack{i=8k+1 \\ k\in\mathbb{N}}}^{N} \mathbf{S}_i \cdot \mathbf{S}_{i+1} + \mathbf{S}_{i+2} \cdot \mathbf{S}_{i+3} + J \sum_{i=1}^{N-4} \mathbf{S}_i \cdot \mathbf{S}_{i+4} \\ & + \alpha \sum_{\substack{i=8k+1 \\ k\in\mathbb{N}}}^{N} K S_{i+4}^z S_{i+7}^z + K S_{i+5}^z S_{i+6}^z + J \mathbf{S}_{i+2} \cdot \mathbf{S}_{i+3}\end{aligned} \tag{4.5}$$

As was the case for the 2-leg ladder, α is a strength parameter which allows us to go from the normal 4-leg ladder to the pruned 4-leg ladder by setting either $\alpha = 1$ or $\alpha = 0$ respectively. We can now proceed to apply the DMRG algorithm to this Hamiltonian. A similar mapping is done with the 3-leg and 5-leg ladders.

In general, when mapping an n-leg ladder system onto a one dimensional chain, given our numbering pattern we see the appearance of long range interactions up to n sites away. Much like how DMRG encodes quantum states as matrix product states, the Hamiltonian is encoded as a matrix product operator which takes the form of a sparse matrix. The sparseness of this matrix is integral to rapid computation. However, long range interactions add off diagonal terms to the Hamiltonian matrix product operator and reduce the sparceness of the matrix. As such, these long range interactions significantly impact the speed of calculations and thus limit the size of systems we can study, particularly for larger ladder systems. This is also one of the key reasons for considering horizontal open boundary conditions, as these would add an interaction term between sites at the start of the chain and sites at the end of the chain.

4.4 ITensor library

To implement the DMRG algorithm, we make use of the ITensor library for C++ [22]. This is a powerful tool which allows us to write down the Hamiltonian as it appears in equations 4.4 and 4.5. This Hamiltonian is then stored as a matrix product operator. We then generate a random matrix product state of $N = nL$ sites, L being the length of the n-leg ladder to act as our initial state. ITensor allows us to then feed this initial state along with the Hamiltonian

MPO into a DMRG algorithm which outputs the approximate ground state and corresponding ground state energy.

The DMRG algorithm used also takes in a number of parameters to determine the accuracy. The first of these is the number of sweeps s. DMRG can be used iteratively, meaning that after feeding the random initial MPS into the algorithm, we obtain an approximate ground state which may not be very good. However, we can take this approximate ground state and use it as an initial state in another iteration of the DMRG algorithm. By repeating this process, we obtain a better approximation of the ground state of the system with each iteration. Each iteration of the DMRG algorithm is called a sweep, thus s defines the number of iterations made. The next parameter is the bond dimension m which dictates the number of singular values kept in the SVD before truncating the remaining singular values.

Typically, a low bond dimension of order 10^2 is used for the first few sweeps. This allows us to rapidly converge from a random initial state to a rough approximation of the ground state. The bond dimension is then steadily increased with each sweep to fine tune the ground state approximation. For most systems, a total of $s = 15$ sweeps with a final bond dimension of $m = 2000$ is enough to provide accurate results while keeping computing times manageable.

Additionally, a truncation error ϵ can be set alongside the bond dimension m. This truncation error is defined by taking the sum of the squared singular values which have been discarded and normalising it with respect to the sum of all squared singular values. For some systems, a similar accuracy can be reached with a smaller bond dimension. Thus, we can set a value for ϵ where if the truncation error becomes smaller than ϵ before reaching the bond dimension, the algorithm will proceed with only the minimum bond dimension necessary to achieve the desired truncation error. Typically, the truncation error is set to be at least 10^{-8}.

The output of the DMRG algorithm is the ground state expressed in matrix product form. With ITensor, we are able to store this ground state and perform calculations on it. One such operation is calculating the string order parameter as defined in chapter 3. We can write down the SOP as given by equation 3.20 as an MPO and use ITensor to calculate the expectation value of the SOP on the ground state as a function of lattice site r.

Chapter 5

Results

In this chapter the various results obtained are presented. To obtain these results, we start by defining the lattice of the model we choose to study, for example the 2-leg ladder or the 4-leg ladder. We then set the size of the system by choosing the length L of the lattice. Thus, the total number of sites on the lattice is given by $N = nL$ where n is the number of legs of the system, for example $N = 4L$ for the 4-leg ladder. Each site is then assigned a random spin 1/2, thus giving us a random initial state of N spins.

On this lattice, we then define our Kitaev-Heisenberg Hamiltonian given by the equation below.

$$H = K \sum_{\gamma \in \langle i,j \rangle} S_i^\gamma S_j^\gamma + J \sum_{\langle i,j \rangle} \mathbf{S}_i \cdot \mathbf{S}_j \tag{5.1}$$

Note that this expression of the Hamiltonian does not change with the different lattices we study. The notation $\langle i, j \rangle$ refers to nearest-neighbour interactions. The S operators refer to $S = 1/2$ spin operators. The parameter γ becomes $\gamma = x, y, z$ depending on the bond type of the Kitaev lattice.

The Hamiltonian is parametrized by setting $K = \sin\phi$ and $J = \cos\phi$, with $\phi \in [0, 2\pi[$. Given this, when $\phi = \frac{\pi}{2}$ or $\frac{3\pi}{2}$, the Hamiltonian reduces to the Kitaev ladder. These two values of ϕ are referred to as the Kitaev points.

In the context of this thesis, we are interested in Hamiltonians where ϕ is set near the Kitaev points $\phi = \frac{\pi}{2}$ and $\phi = \frac{3\pi}{2}$. As such, the system closely resembles a Kitaev Hamiltonian, but with a slight Heisenberg perturbation which becomes more and more important as we

move away from the Kitaev points.

Once our system is defined with a random initial state and a Hamiltonian with a set value of ϕ, we encode the initial state as a matrix product state $|\psi_0\rangle$ and the Hamiltonian as a matrix product operator $\hat{H}$. We then proceed to use the DMRG process described in chapter 4 to find the ground state $|\psi\rangle$ of the specific Hamiltonian from the random initial state. This DMRG calculation is achieved using the ITensor library in C++ [22].

After finding the ground state of the system, we then proceed to calculate the string order parameter $O^z(r)$ using equation 3.20 and the method described in chapter 4. In order to compare the string order parameter for different values of ϕ and explore the effect of the Heisenberg term on the string order parameter, we define a new parameter O^z. Since we are interested in long-range order, we are interested in the values of $O^z(r)$ as r grows large. For this reason, we define the parameter O^z as follows :

$$O^z = \sqrt{|O^z\left(3L/4\right)|_{max}} \tag{5.2}$$

where $|O^z\left(3L/4\right)|_{max}$ is the maximal value of $O^z(r)$ in the vicinity of $r = 3L/4$, with L being the length of the lattice. O^z is defined as such in order to avoid boundary effects at $r = L$ while still keeping r large.

With this definition, we obtain a unique value of O^z for each Hamiltonian defined by ϕ. We can then vary the value of ϕ around the Kitaev points to see how this affects O^z. We can now proceed to calculating O^z around the Kitaev points for the various ladder models.

5.1 String order parameter in the 4-leg ladder

In the study by Catuneanu, Sorensen, and Kee [17], they looked at how O^z changes with ϕ around the Kitaev points for the 2-leg ladder. To build on their results, we are doing the same analysis but on the 4-leg ladder to be able to compare with their results. In this section, we present the values of O^z as a function of ϕ around the Kitaev points for various system lengths L of the 4-leg ladder.

We first look at O^z as defined by equation 5.2 around the antiferromagnetic point $\phi = \pi/2$. We can also define $\chi_E = -\partial_\phi^2 e_0$ as the second derivative of the ground state energy per site with respect to ϕ. This lets us define phase boundaries of the second order phase

transition by associating the boundaries with maximums of χ_E.

Figure 5.1 shows results obtained by DMRG on the 4-leg ladder of different lengths around the antiferromagnetic point at $\phi = \pi/2$. For each point, we set a value of ϕ, thus setting specific values of K and J in the Hamiltonian 5.1. From there, a random initial state is generated to which the DMRG algorithm is applied in order to find the ground state and the corresponding ground state energy.

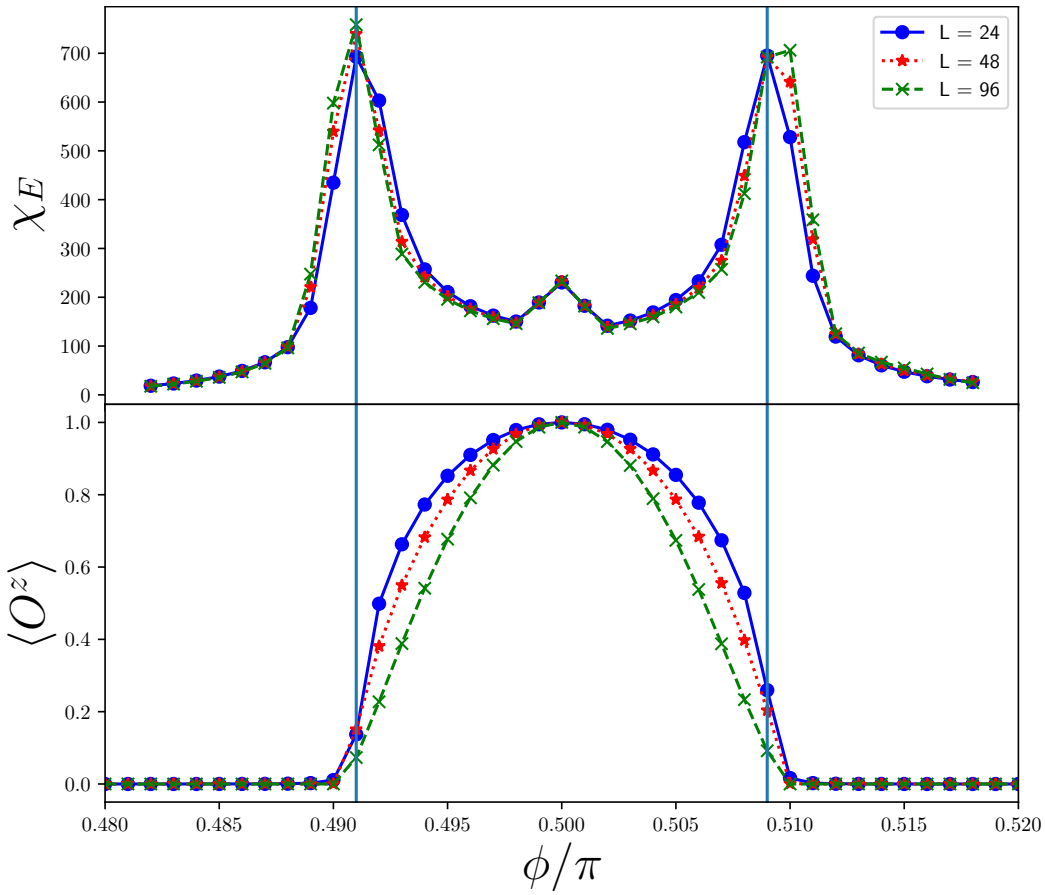

Figure 5.1: 4-leg ladder around antiferromagnetic point. L represents the length of each leg. The DMRG parameters used for each simulation are : For L = 24 and L=48, the largest bond dimension is $m = 1500$ and the number of DMRG sweeps done is $s = 20$. For L = 96, the largest bond dimension is $m = 600$ and the number of DMRG sweeps done is $s = 10$. The vertical lines correspond to the maximums of χ_E which occur at $\phi_1 = 0.491$ and $\phi_2 = 0.509$

From this figure, we notice that for $\phi \in [\phi_1, \phi_2]$, where $\phi_1 = 0.491$ and $\phi_2 = 0.509$,

the string order parameter O^z is non-zero. When ϕ falls outside of this range, the SOP falls to zero. Since ϕ_1 and ϕ_2 correspond to maximums of χ_E, this indicates the presence of a second-order phase transition at those points. We find that the string order parameter is non-zero around the antiferromagnetic Kitaev point, but falls to zero after the phase transition. The SOP is exactly 1 at the Kitaev point. This is an indicator of long range order within the antiferromagnetic Kitaev phase of the 4-leg Kitaev-Heisenberg ladder.

Comparing the results for various system sizes, we see that the graphs of χ_E are very similar for each value of L. The graphs for O^z are also similar in shape, but we note that for each value of ϕ, O^z gets slightly smaller as L increases.

Let us shift our focus to the ferromagnetic point now. We repeat the same analysis on the 4-leg ladder but look at values of ϕ close to $\phi = 3\pi/2$. Figure 5.2 shows O^z and χ_E as functions of ϕ around the ferromagnetic point.

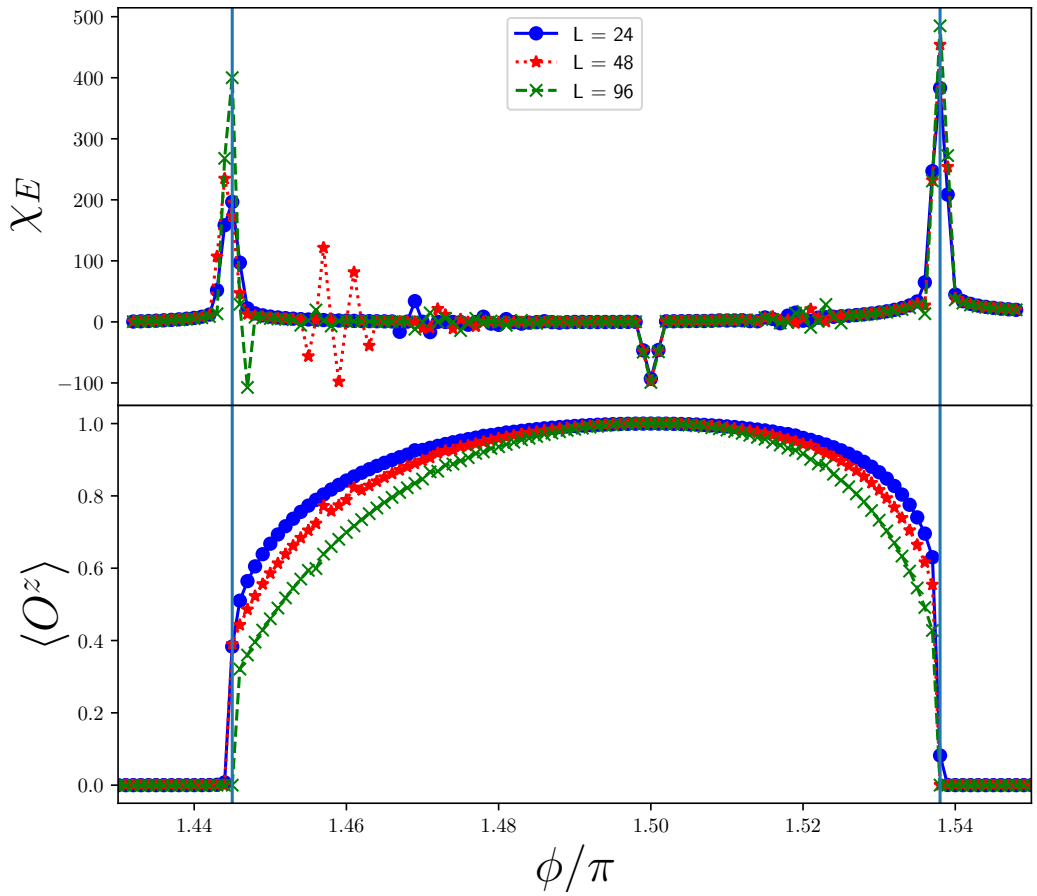

Figure 5.2: 4-leg ladder around ferromagnetic point. L represents the length of each leg. The DMRG parameters used for each simulation are : For L = 24 and L = 48, the largest bond dimension is $m = 1500$ and the number of DMRG sweeps done is $s = 20$. For L = 96, the largest bond dimension is $m = 600$ and the number of DMRG sweeps done is $s = 10$. The vertical lines correspond to the maximums of χ_E which occur at $\phi_1 = 1.445$ and $\phi_2 = 1.538$

We see here once again the presence of a second order phase transition corresponding with the string order parameter. When $\phi \in [\phi_1, \phi_2]$ with $\phi_1 = 1.445$ and $\phi_2 = 1.538$, the string order parameter is non-zero and when ϕ falls outside of this range the SOP drops to zero. Similarly to the antiferromagnetic point, the system size seems to have little effect on the shape of the SOP graph but having slightly smaller values of O^z as L increases.

We must point out the presence of scattering around $\phi = 1.46$ when $L = 48$. While the nature of this scattering is unknown, we believe it is due to some difficulties in finding the true ground state by the DMRG algorithm due to the presence of low lying excited states.

5.2 Comparison of 2-leg ladder and 4-leg ladder

With these results for the 4-leg ladder, we can now compare them with the results from the 2-leg ladder obtained by Catuneanu, Sørensen, and Kee [17]. Using our DMRG algorithm, we have reproduced their results for the 2-leg ladder. The figure below shows χ_E and O^z as functions of ϕ around the antiferromagnetic point for both the 4-leg and the 2-leg ladders.

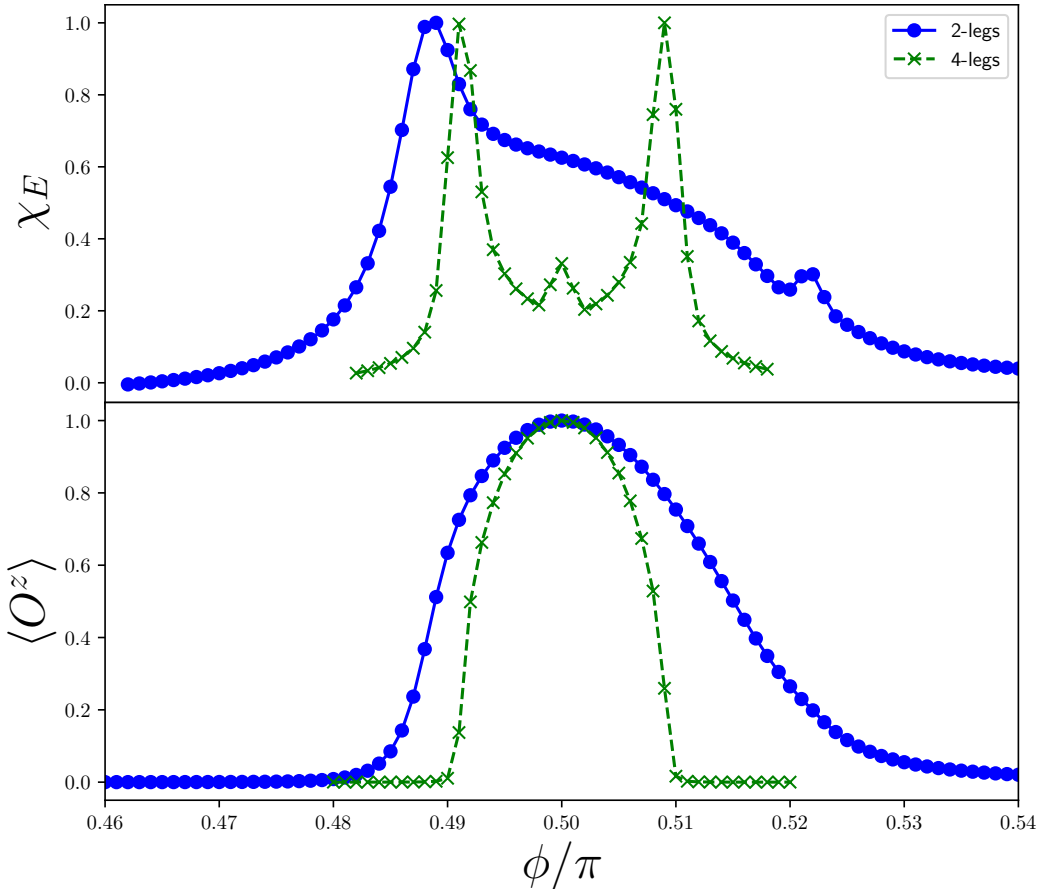

Figure 5.3: Comparison of χ_E and O^z around the antiferromagnetic point for the 2-leg and 4-leg ladders. For the 2-leg ladder, we studied a ladder of length $L = 24$ with the following DMRG parameters : largest bond dimension of $m = 1500$ and $s = 15$ sweeps. For the 4-leg ladder, we studied a ladder of length $L = 24$ with the following DMRG parameters : largest bond dimension of $m = 1500$ and $s = 15$ sweeps.

Comparing the two curves, the most notable difference is where the phase transition happens. For the 2-leg ladder, we have values of $\phi_1^{2leg} = 0.489$ and $\phi_2^{2leg} = 0.522$, while for

the 4-leg ladder we have $\phi_1^{4leg} = 0.491$ and $\phi_2^{4leg} = 0.509$. As such, the antiferromagnetic Kitaev phase where O^z is non-zero is narrower for the 4-leg ladder. The results obtained for the 2-leg ladder agree with the results obtained by Catuneanu, Sorensen, and Kee [17].

Similarly, we can also compare these results for the ferromagnetic point. The figure below shows a comparison of χ_E and O^z between the 2-leg and the 4-leg ladder around the ferromagnetic point.

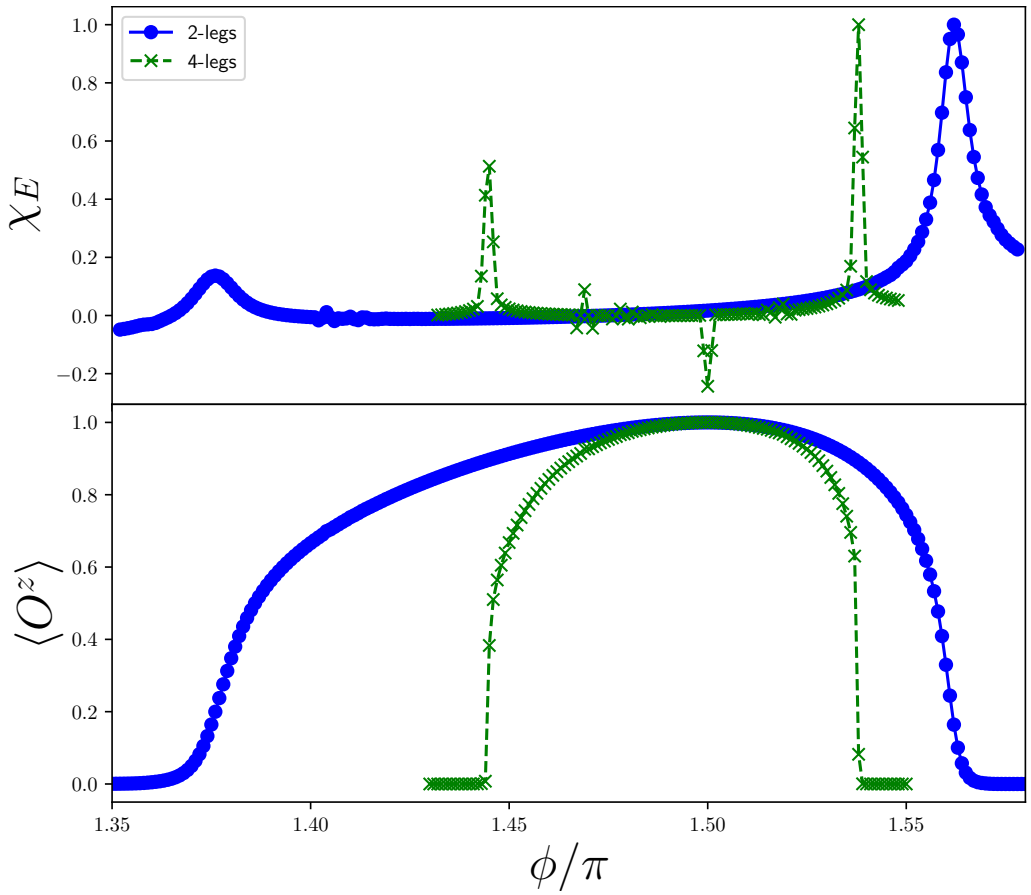

Figure 5.4: Comparison of χ_E and O^z around the ferromagnetic point for the 2-leg and 4-leg ladders. For the 2-leg ladder, we studied a ladder of length $L = 24$ with the following DMRG parameters : largest bond dimension of $m = 1500$ and $s = 15$ sweeps. For the 4-leg ladder, we studied a ladder of length $L = 24$ with the following DMRG parameters : largest bond dimension of $m = 1500$ and $s = 15$ sweeps.

Here the phase transitions occur at $\phi_1^{2leg} = 1.376$ and $\phi_2^{2leg} = 1.562$ for the 2-leg ladder

and at $\phi_1^{4leg} = 1.445$ and $\phi_2^{4leg} = 1.538$ for the 4-leg ladder. Again, the ferromagnetic Kitaev phase is narrower for the 4-leg ladder. Once again, the results obtained for the 2-leg ladder match closely the results obtained by Catuneanu, Sørensen, and Kee [17].

For both the antiferromagnetic and ferromagnetic Kitaev points, we find that while the 4-leg ladder shows the existence of a non-zero string order parameter which survives the Heisenberg interaction, the window in which the SOP survives is smaller in the 4-leg ladder. Along with this, the results for χ_E show that the AFK and FK phases are both smaller in the 4-leg ladder compared to the 2-leg ladder.

5.3 Oz vs r

So far, we have only looked at the behaviour of the string order parameter $\langle O^z(r)\rangle$ by finding the maximum value of the SOP at long range for each value of ϕ and comparing these maximums as we vary ϕ. Let us now take a closer look at the behaviour of the string order parameter itself as a function of lattice site r for both the 2-leg and 4-leg ladder for specific values of ϕ. At the Kitaev points of $\phi = 0.5\pi$ and $\phi = 1.5\pi$, the SOP is exactly 1 even at large values of r in both the 2-leg and the 4-leg ladders. Given this, it is more interesting to look at the behaviour of $O^z(r)$ at points inside the phase where O^z is non-zero, but not exactly at the Kitaev points.

Starting at the antiferromagnetic point for the 2-leg ladder, we set $\phi = 0.51\pi$. From figure 5.3, we see that at this point, the 2-leg ladder is in the AFK phase and O^z is non-zero with a value of around $O^z_{2-leg}(0.51\pi) = 0.755$. Let us have a look at the behaviour of $O^z(r)$ at this point.

The figure below shows the string order parameter $\langle O^z(r)\rangle$ as defined by equation 3.20 as a function of lattice site r on the 2-leg ladder of length $L = 96$.

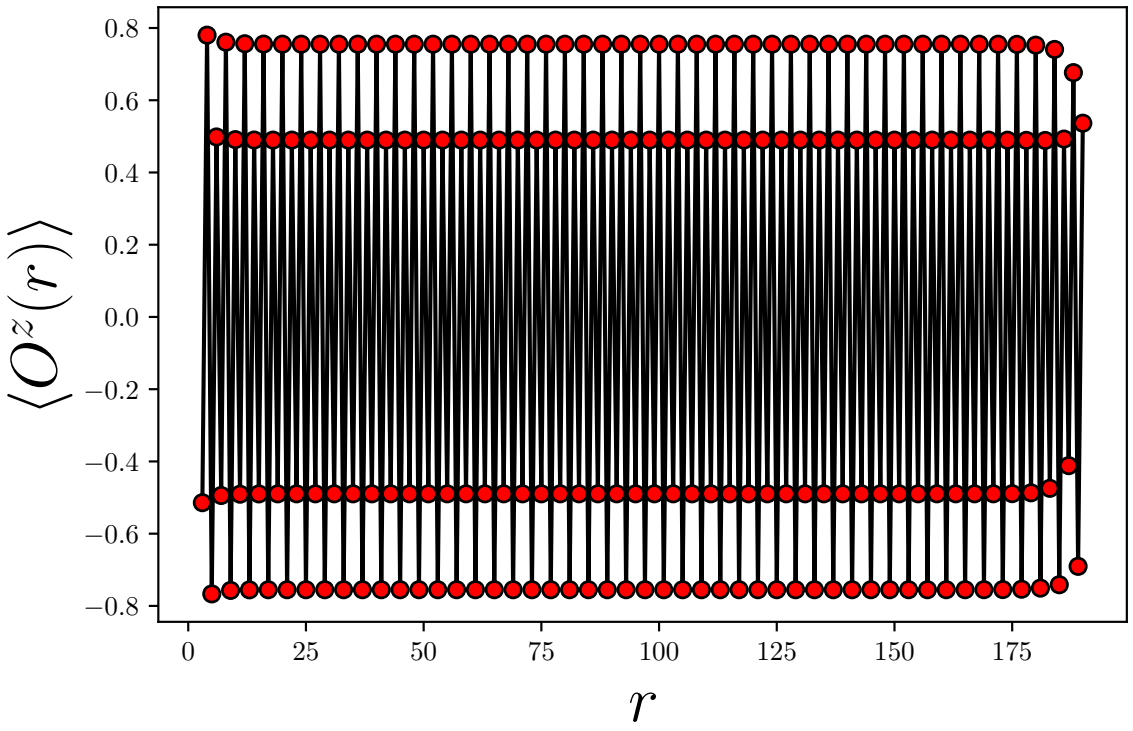

Figure 5.5: String order parameter $\langle O^z(r)\rangle$ as a function of lattice site r on the 2-leg ladder of length $L = 96$. This figure shows results obtained for $\phi = 0.51\pi$ near the antiferromagnetic point. The results are obtained from DMRG calculations with a typical truncation error of $10^{(-11)}$.

From this figure, we see that not only does $O^z(r)$ alternate between positive and negative values, but the values are grouped in four distinct lines. The negative values are due to the presence of $(-1)^{\lfloor (r+1)/2 \rfloor}$ in equation 3.20 while the presence of four distinct groups arises from the geometry of the Kitaev model. Due to the alternating x and y bonds, there are essentially four unique sites which are repeated periodically to form the 2-leg ladder. Each distinct line in figure 5.5 corresponds to a distinct family of sites.

At this value of $\phi = 0.51$ for the 2-leg ladder, the measured value of O^z using equation 5.2 is $O^z = 0.755156$. From figure 5.5, we see that this value is associated with the top most group of points. Isolating this group of values, it is interesting to take a closer look and see if we can extrapolate a behaviour that we can then extend to larger lattices. The figure below shows only the top row of points from figure 5.5. An exponential fit of the form $a\mathrm{e}^{(-x/b)} + c$

is plotted along with the points.

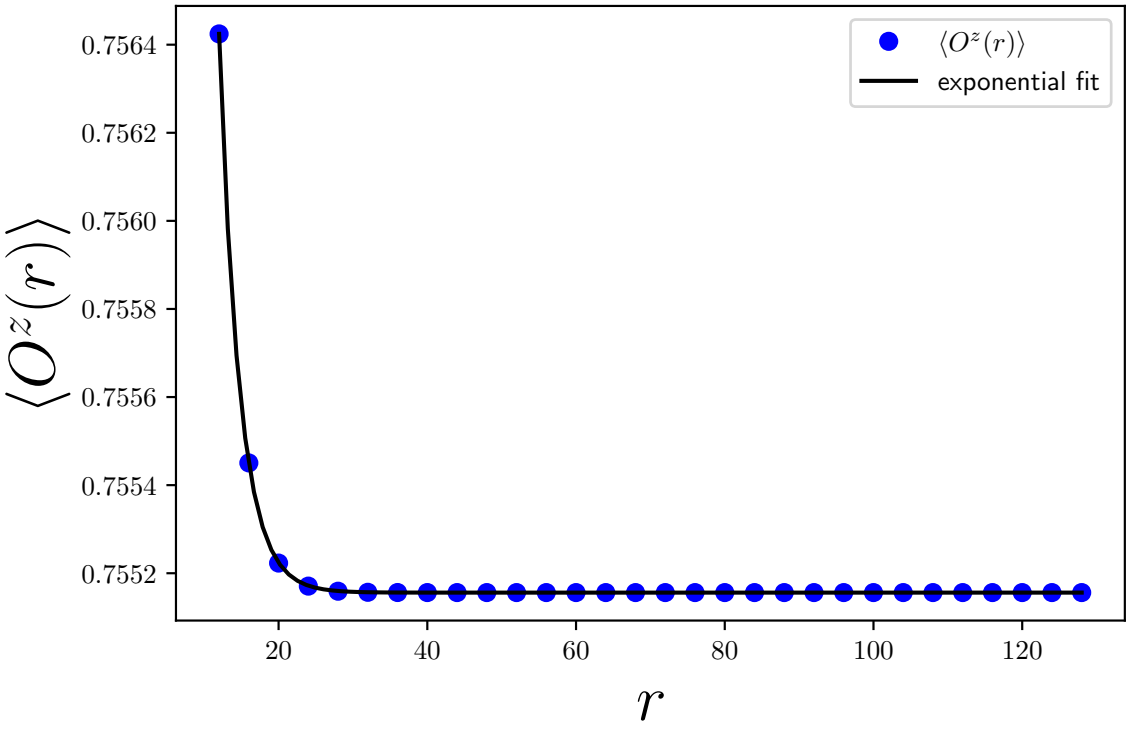

Figure 5.6: String order parameter $\langle O^z(r)\rangle$ as a function of lattice site r on the 2-leg ladder of length $L = 96$. This figure shows results obtained for $\phi = 0.51\pi$ near the antiferromagnetic point. The exponential fit is given by the equation $f(x) = ae^{(-x/b)} + c$ with $a = 0.1021 \pm 0.0003$, $b = 2.735 \pm 0.002$, and $c = 0.75515600 \pm 0.00000006$

To obtain this fit, we truncate the first few and last few values to minimise boundary effects. We see remarkable agreement between the values of $c = 0.75515600 \pm 0.00000006$ and $O^z = 0.755156$. This could indicate the presence of long-range order in a macroscopic model of the 2-leg Kitaev-Heisenberg ladder with a length much larger than $L = 96$.

Let's compare this with the 4-leg ladder. The figure below shows a plot of $O^z(r)$ on the 4-leg ladder of length $L = 96$ at $\phi = 0.504\pi$ near the antiferromagnetic point. At this point, the measured value for O^z is $O^z = 0.789193$.

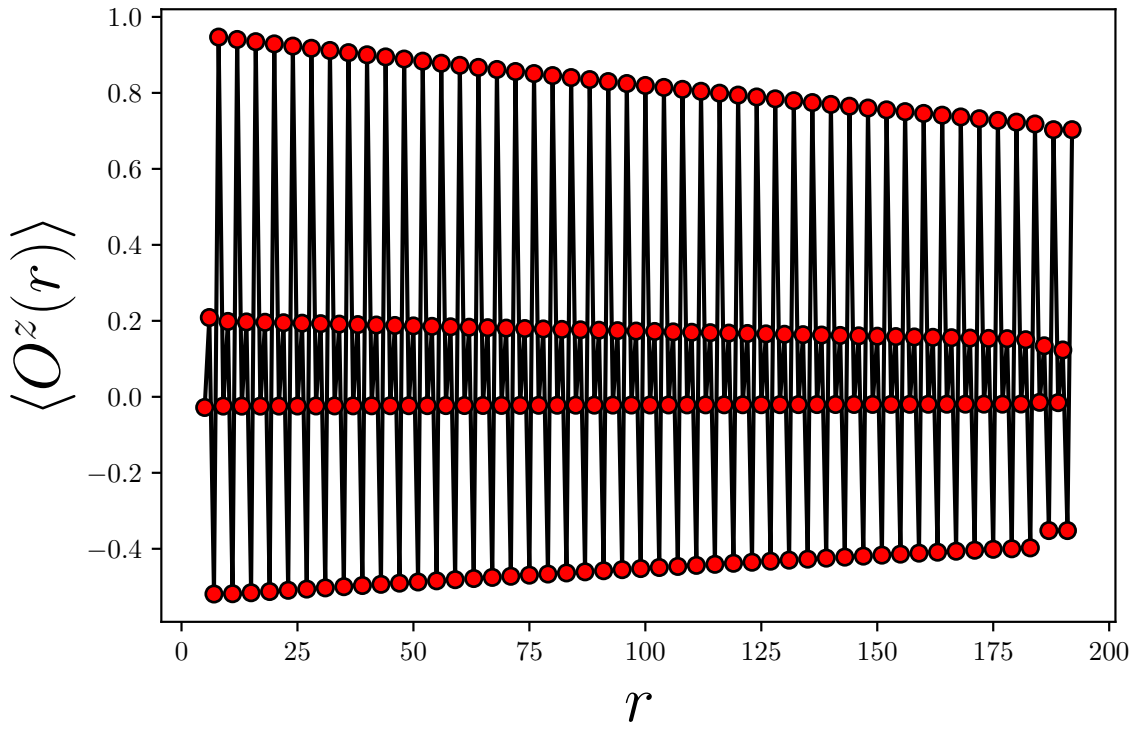

Figure 5.7: String order parameter $\langle O^z(r) \rangle$ as a function of lattice site r on the 4-leg ladder of length $L = 96$. This figure shows results obtained for $\phi = 0.504\pi$ near the antiferromagnetic point. The results are obtained from DMRG calculations with a typical truncation error of $10^(-11)$.

Similarly to the 2-leg ladder, the points are separated in 4 groups. However, the top most group is sloping down, as opposed to the top most group in figure 5.5 where it seems to be constant. This could indicate that our results of O^z for the 4-leg ladder are due to the relatively short values of L when compared to a macroscopic model of the 4-leg ladder. Indeed, figure 5.1 shows that O^z decreases slightly as L increases and it is unclear what happens for large values of L. To investigate this further, as we did for the 2-leg ladder, let's try fitting an exponential to the top most group of values of $\langle O^z(r) \rangle$. The figure below shows the result of this exponential fit.

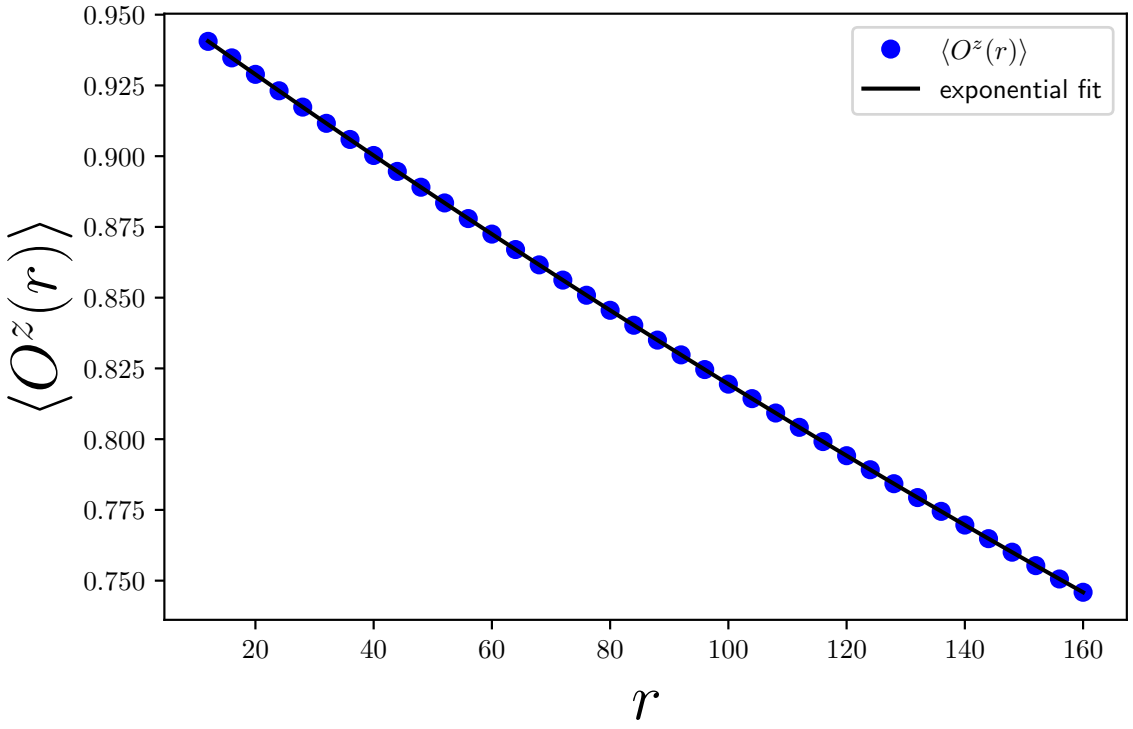

Figure 5.8: String order parameter $\langle O^z(r)\rangle$ as a function of lattice site r on the 4-leg ladder of length $L = 96$. This figure shows results obtained for $\phi = 0.504\pi$ near the antiferromagnetic point. The exponential fit is given by the equation $f(x) = a\mathrm{e}^{(-x/b)} + c$ with $a = 0.9605 \pm 0.0007$, $b = 639.6 \pm 0.5$, and $c = -0.0021 \pm 0.0007$

We see here that instead of going to a constant, the points are much more linear. Additionally, looking at the values for the a, b, and c parameters of the exponential fit, we see they are much different than the values obtained for the 2-leg ladder. Most notably, we obtain a value of $c = -0.0021$. This is in stark opposition to the 2-leg result where the value of c was in close agreement with O^z. This could indicate that no long-range order is present in the 4-leg system when looking at macroscopic system sizes.

However, we have only looked at one specific value of ϕ for both the 2-leg and 4-leg ladders. We can repeat this analysis of fitting an exponential to the top most family of values in $O^z(r)$ for other values of ϕ and see how the parameters a, b, and c behave. For each value of ϕ in the AFK phase, we have a set of values for $O^z(r)$. We fit an exponential of the form $a\mathrm{e}^{-x/b} + c$ to this set of data. We repeat this process for each value of ϕ around the antiferro-

magnetic point.

The figure below shows the results of these fits on the 2-leg ladder. The fit parameters a, b, and c are plotted as a function of ϕ.

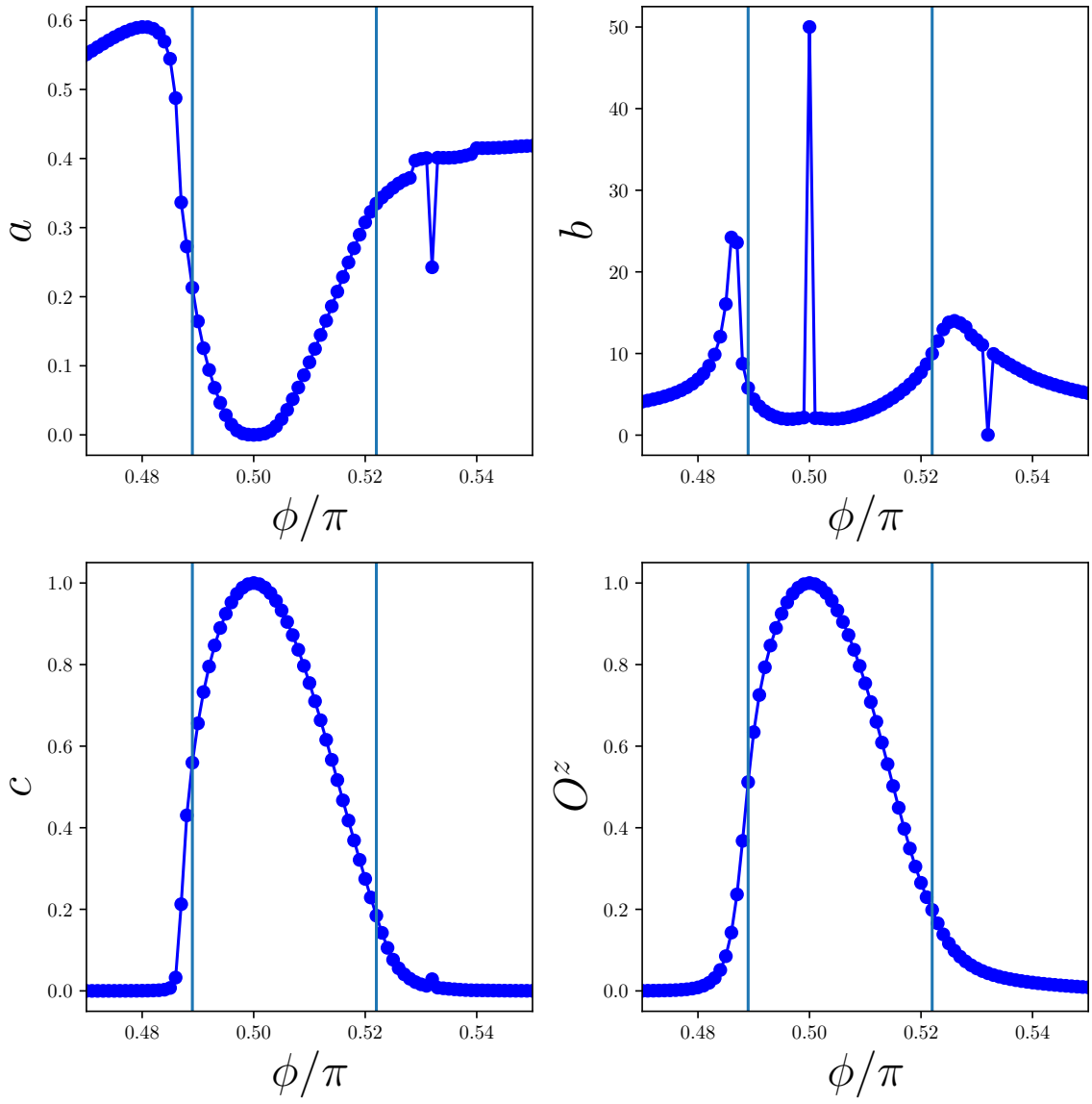

Figure 5.9: Exponential fit parameters for $O^z(r)$ on the 2-leg ladder around the antiferromagnetic point. For each value of ϕ an exponential fit of the form $ae^{-x/b} + c$ is done to the associated values of $O^z(r)$. The first three panels show the fit parameters a, b, and c respectively as functions of ϕ. The fourth panel shows O^z as given by equation 5.2 as a function of ϕ.

Of particular interest are the results obtained for ϕ between the blue vertical lines. These lines denote the AFK phase between maximums of χ_E. In the AFK phase, we see that a ranges between 0 and 1 while b ranges between 0 and 10 with the exception of $\phi = 0.5\pi$.

However, at exactly the Kitaev point $\phi = 0.5\pi$, $O^z(r)$ is exactly 1 for all values of r. As such, the exponential fit returns a value of $a = 0$ and $c = 1$, thus killing the exponential term and making the value of b at that point meaningless.

We can clearly see an agreement between the values of c and O^z for all values of ϕ within the AFK phase. This indicates that as r grows along the lattice, $O^z(r)$ goes to a constant. Thus this is a good indicator that $O^z(r)$ persists as $r \to \infty$ on a macroscopic system of the 2-leg ladder with a much larger value of L.

Let us repeat this analysis on the 4-leg ladder around the antiferromagnetic point to see if these results hold. The figure below shows the results of the same analysis done of the 4-leg ladder of length $L = 48$.

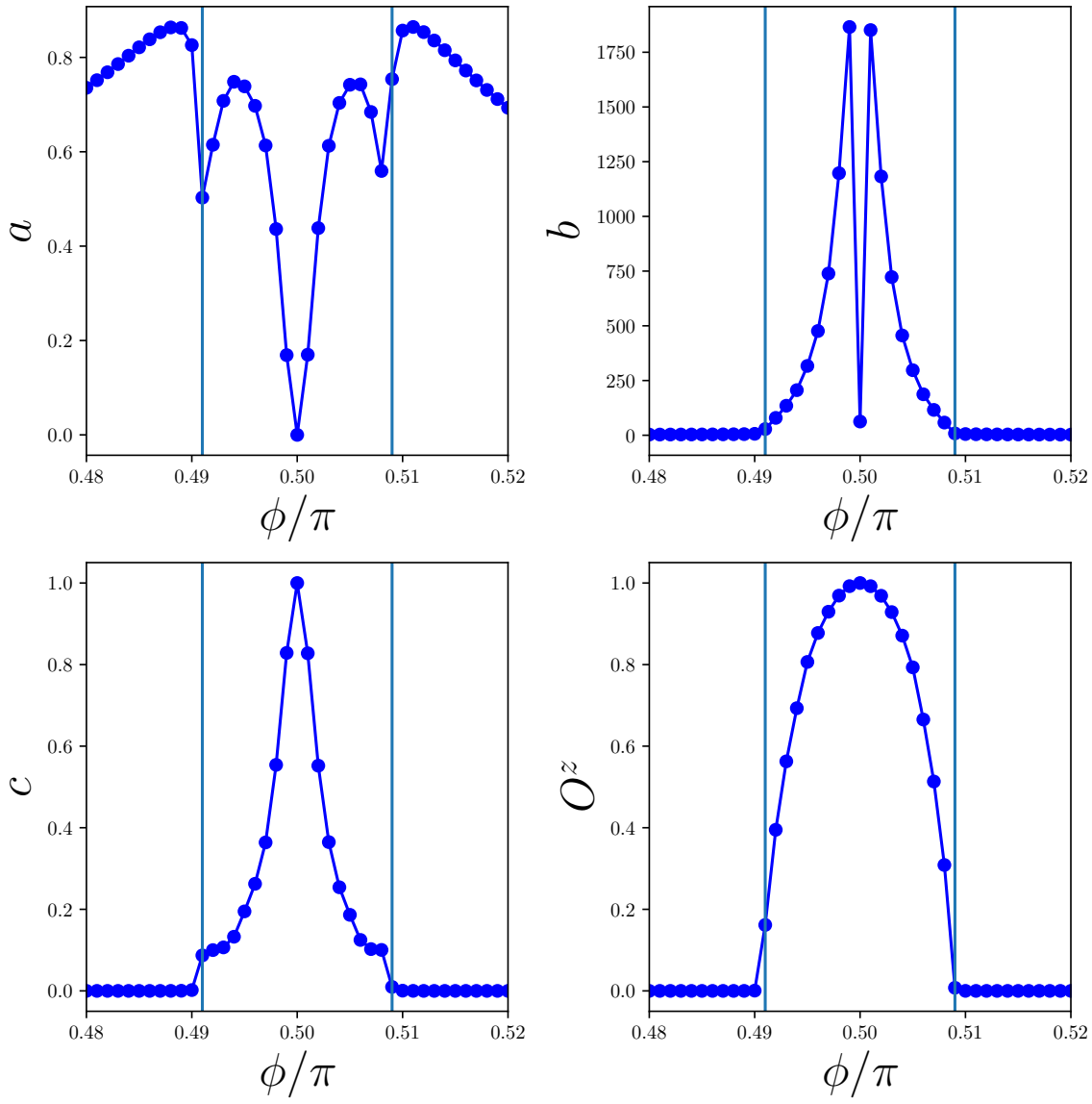

Figure 5.10: Exponential fit parameters for $O^z(r)$ on the 4-leg ladder around the antiferromagnetic point. For each value of ϕ an exponential fit of the form $ae^{-x/b} + c$ is done to the associated values of $O^z(r)$. The first three panels show the fit parameters a, b, and c respectively as functions of ϕ. The fourth panel shows O^z as given by equation 5.2 as a function of ϕ.

Here we see a much different picture than in the 2-leg case. Again focusing our attention to the points between the blue vertical lines corresponding to the AFK phase, we see that for a, while the values are still between 0 and 1, the shape is much different. While a is still zero

at exactly $\phi = 0.5\pi$, we see a symmetric function around $\phi = 0.5\pi$ and two local maximums within the AFK phase. For b, the values are much larger, going up to the hundreds and thousands. Once again, at exactly $\phi = 0.5\pi$ we have $a = 0$ making the value of b meaningless at that point.

Lastly, c shows a stark difference when compared to O^z. While we still see $c = 1$ at the Kitaev point, c then quickly drops. This is in contrast with the 2-leg ladder where c behaved almost identically to O^z. This could be an indication that while the 2-leg ladder shows long range order even as $r \to \infty$, the 4-leg ladder does not. To truly answer this question, larger system sizes of the 4-leg ladder would need to be studied to see if O^z also eventually vanishes with large values of L.

So far in our analysis, we have only focused on the antiferromagnetic point. We can repeat our analysis at the ferromagnetic point and see if the system behaves differently. Starting with the 2-leg ladder, we take a look at the behaviour of $O^z(r)$ at $\phi = 1.40\pi$. At this value of ϕ, we have $O^z = 0.6709$ as calculated by equation 5.2.

The figure below shows the behaviour of the string order parameter $\langle O^z(r) \rangle$ as a function of lattice site r on the 2-leg ladder on length $L = 96$ close to the ferromagnetic point.

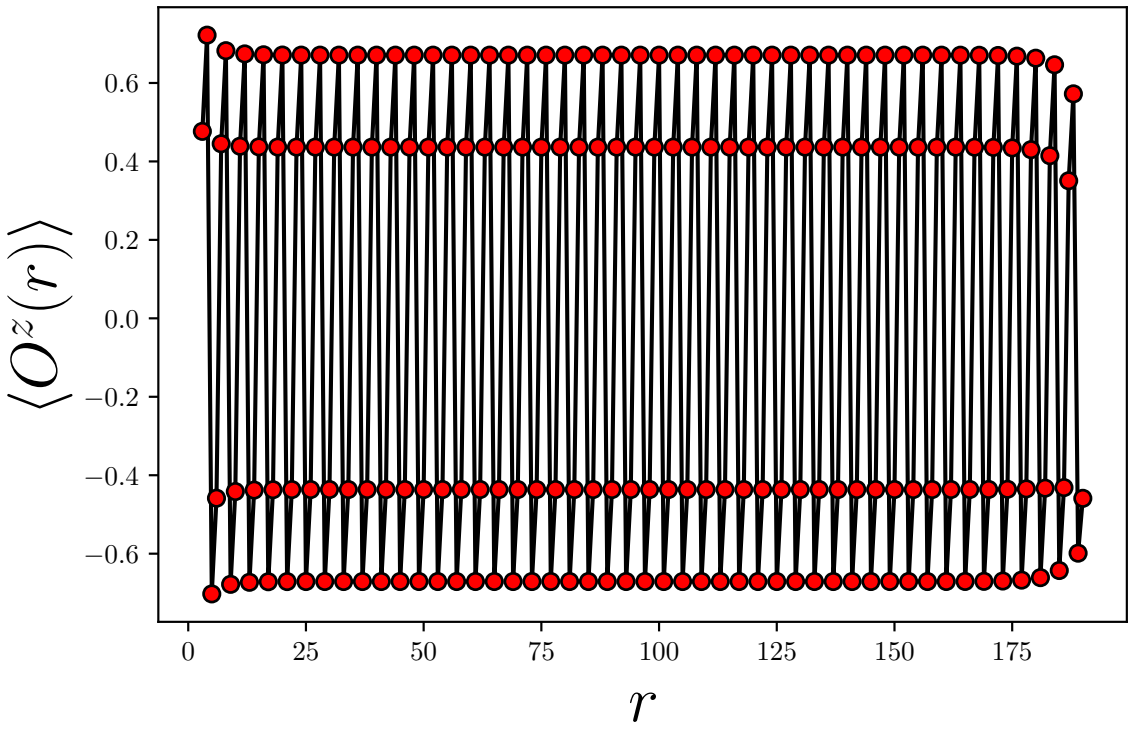

Figure 5.11: String order parameter $\langle O^z(r) \rangle$ as a function of lattice site r on the 2-leg ladder of length $L = 96$. This figure shows results obtained for $\phi = 1.40\pi$ near the ferromagnetic point. The results are obtained from DMRG calculations with a typical truncation error of $10^(-11)$.

Here, similarly to the antiferromagnetic point from figure 5.5, we see the values of $O^z(r)$ forming four distinct groups with the top most group seemingly holding a constant value. We repeat our exponential fit $a\mathrm{e}^{-x/b} + c$ on this top most group of values. The figure below shows the result of the exponential fit.

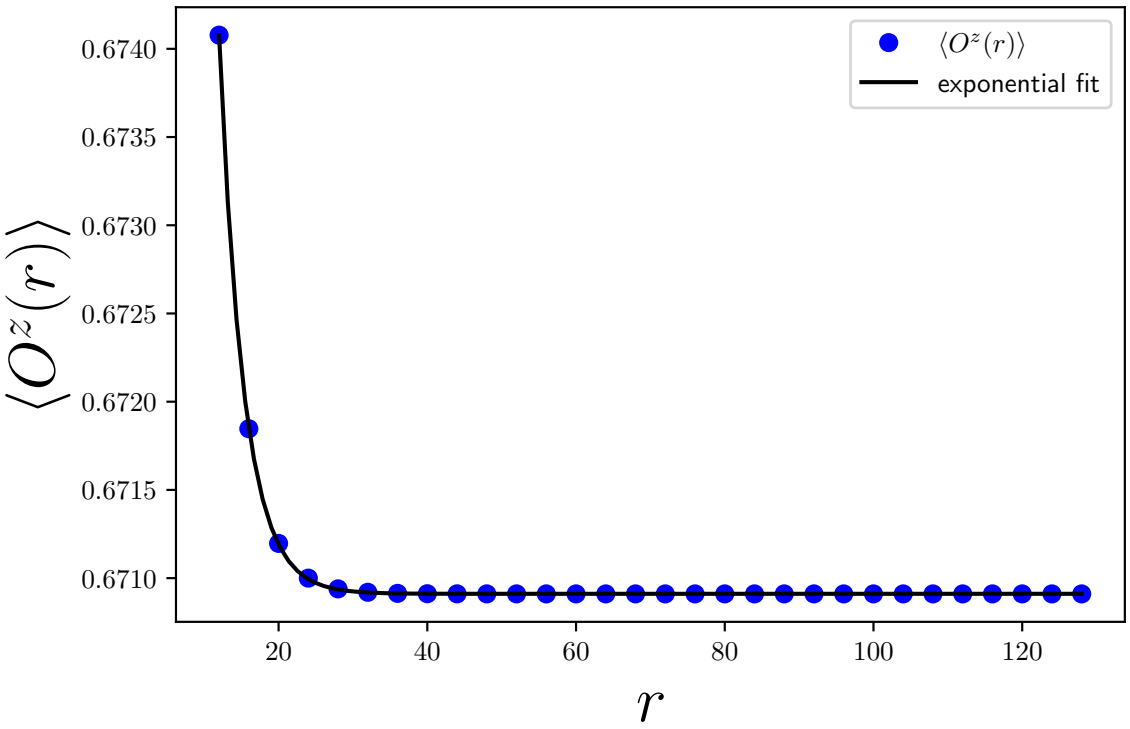

Figure 5.12: String order parameter $\langle O^z(r)\rangle$ as a function of lattice site r on the 2-leg ladder of length $L = 96$. This figure shows results obtained for $\phi = 1.40\pi$ near the ferromagnetic point. The exponential fit is given by the equation $f(x) = ae^{-x/b} + c$ with $a = 0.1205 \pm 0.0007$, $b = 3.297 \pm 0.005$, and $c = 0.6709112 \pm 0.0000004$.

Once again here we see good agreement between the exponential fit and the data. Notably, the value of $c = 0.6709112$ is in good agreement with the value of $O^z = 0.6709$.

Now we can take a look at the string order parameter on the 4-leg ladder close to the ferromagnetic point. Here we set $\phi = 1.465\pi$. At this point for the 4-leg ladder, we have a value of O^z given by $O^z = 0.781572$. Let's see how the string order parameter behaves as a function of lattice site r at this point.

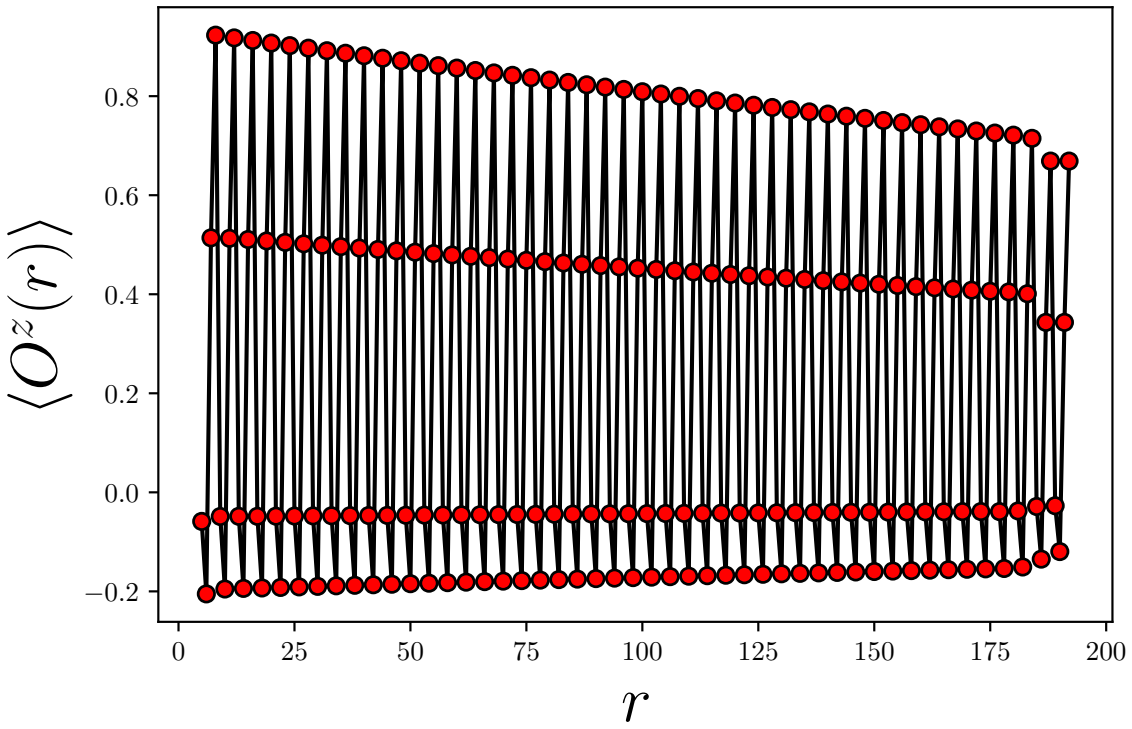

Figure 5.13: String order parameter $\langle O^z(r)\rangle$ as a function of lattice site r on the 4-leg ladder of length $L = 48$. This figure shows results obtained for $\phi = 1.465\pi$ near the ferromagnetic point. The results are obtained from DMRG calculations with a typical truncation error of $10^(-11)$.

Immediately we see that, similarly to the antiferromagnetic case, $O^z(r)$ does not go to a constant and behaves much more linearly in the case of the 4-leg ladder. Nevertheless, let's take a closer look with our exponential fit of the top most family of values.

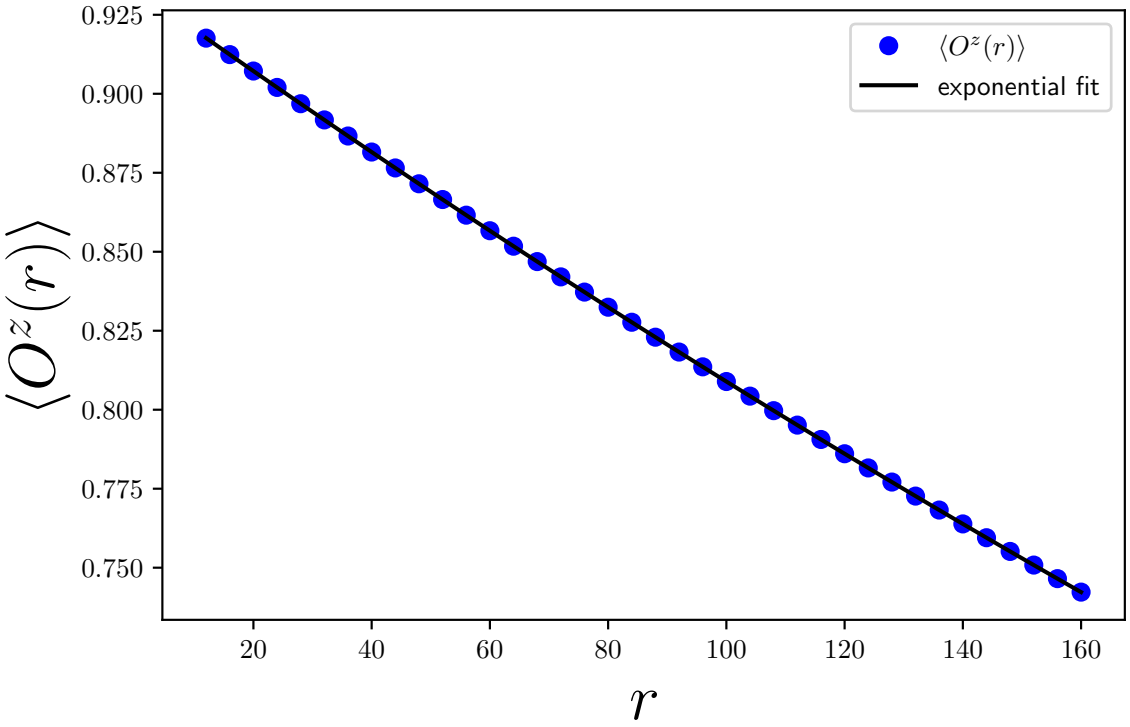

Figure 5.14: String order parameter $\langle O^z(r) \rangle$ as a function of lattice site r on the 4-leg ladder of length $L = 48$. This figure shows results obtained for $\phi = 1.465\pi$ near the ferromagnetic point. The exponential fit is given by the equation $f(x) = a \exp(-x/b) + c$ with $a = 0.9353 \pm 0.0006$, $b = 699.3 \pm 0.5$, and $c = -0.0018 \pm 0.0006$

As can be seen from the value of $c = -0.0018$, in the 4-leg case O^z does not seem to go to a constant as $r \to \infty$ for values close to the ferromagnetic Kitaev point and instead seems to go to zero. However, we have only looked at a single value of ϕ. As we did for the antiferromagnetic Kitaev point, we repeat this exponential fit for each set of values $\langle O^z(r) \rangle$ associated with values of ϕ inside the FK phase. The next figure shows the resulting values of a, b, and c obtained from the exponential fit of $\langle O^z(r) \rangle$ on the 2-leg ladder of length $L = 96$ as functions of ϕ close to the ferromagnetic Kitaev point.

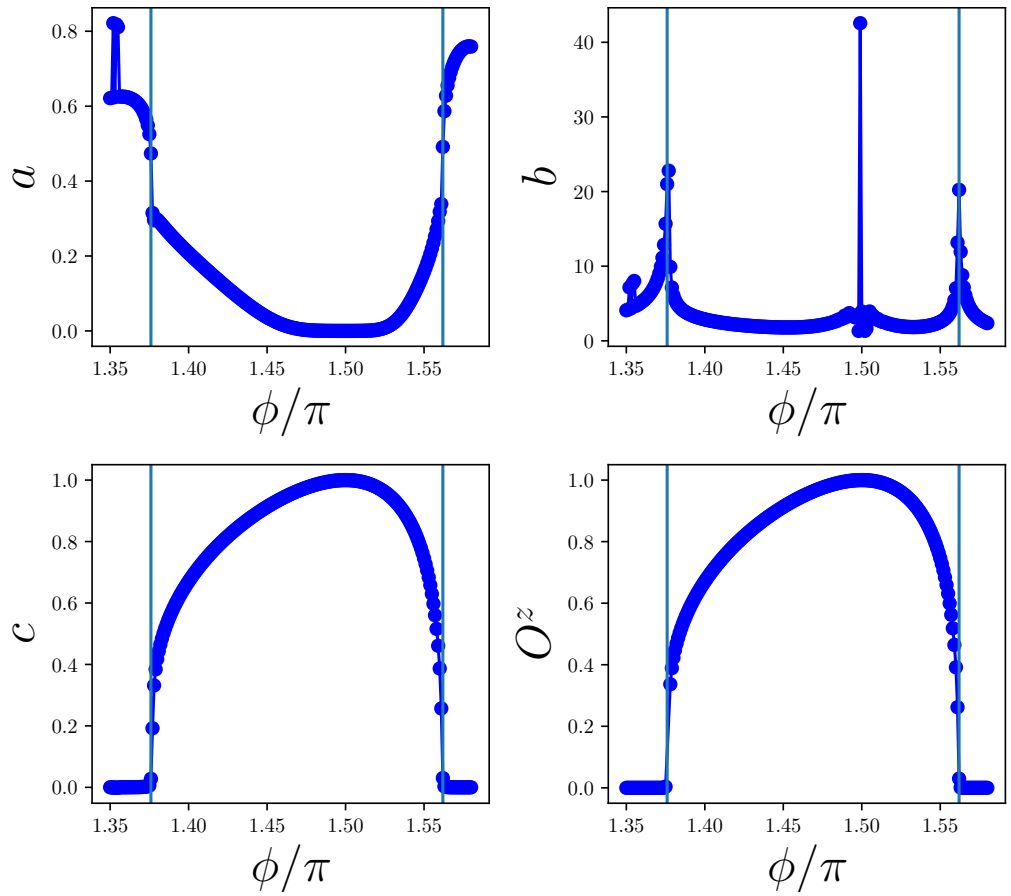

Figure 5.15: Exponential fit parameters for $O^z(r)$ on the 2-leg ladder around the ferromagnetic point. For each value of ϕ an exponential fit of the form $ae^{-x/b} + c$ is done to the associated values of $O^z(r)$. The first three panels show the fit parameters a, b, and c respectively as functions of ϕ. The fourth panel shows O^z as given by equation 5.2 as a function of ϕ.

For the 2-leg ladder, we see a good agreement between the fit parameter c and the values of O^z. In much the same way as for the analysis of the AFK phase, the blue vertical lines denote the FK phase between maximums of χ_E. We see that these also correspond to maximums of the fit parameter b. We also notice that as we get closer to the ferromagnetic Kitaev point at $\phi = 3\pi/2$, the values of a become very close to 0, thus killing the exponential term and leaving only the constant term c. At exactly $\phi = 3\pi/2$, the value of b becomes large, however this is meaningless since at this point we have exactly $a = 0$ and $c = 1$ thus killing the exponential term.

We repeat this analysis of the exponential fit on values of $\langle O^z(r)\rangle$ for the 4-leg ladder of length $L = 48$. Figure 5.16 shows the results obtained.

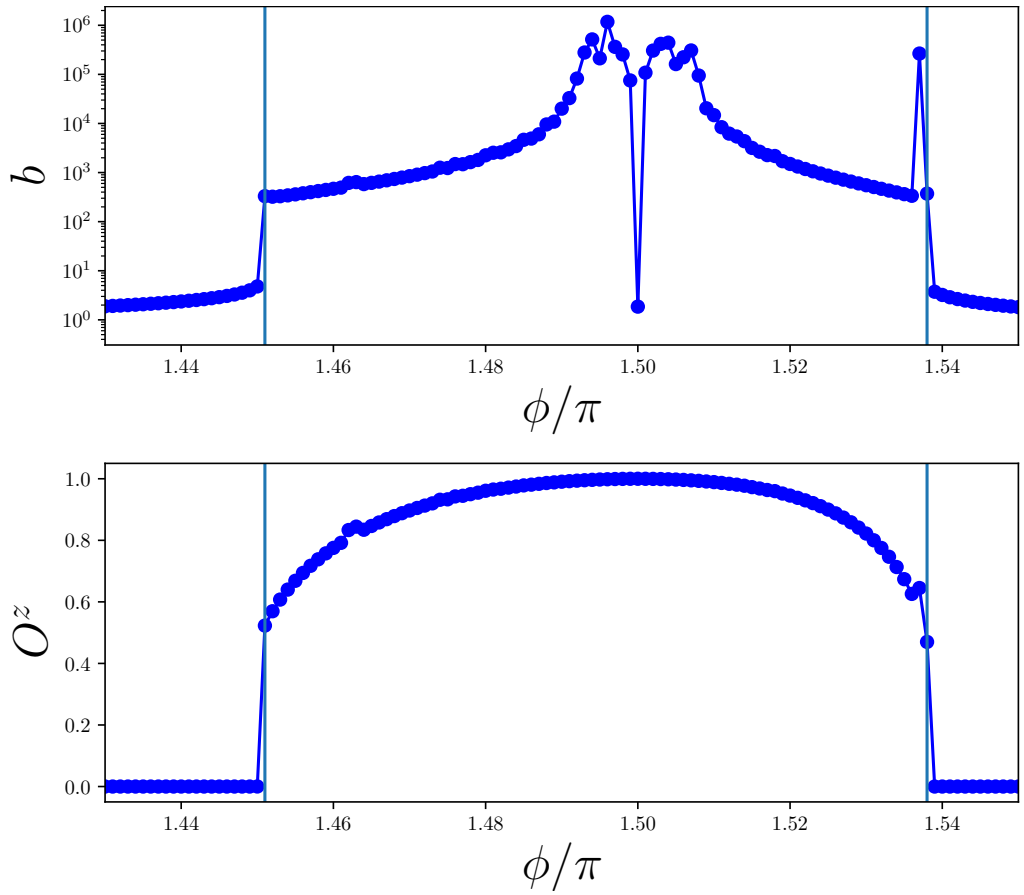

Figure 5.16: Exponential fit parameters for $O^z(r)$ on the 4-leg ladder around the ferromagnetic point. For each value of ϕ an exponential fit of the form $ae^{-x/b} + c$ is done to the associated values of $O^z(r)$. The first panel show the fit parameter b as a function of ϕ on a logarithmic scale. The fourth panel shows O^z as given by equation 5.2 as a function of ϕ.

In figure 5.16, we only show the values of the fit parameter b. The exponential fits for the ferromagnetic point of the 4-leg ladder proved to be difficult and produce inconsistent results. However, it is still interesting to look at the values of b obtained. When doing the exponential fits, the values of b become very large, especially close to the Kitaev point. This first panel in figure 5.16 is shown on a logarithmic scale to better showcase the large values of b. Inside the spin liquid phase, we see that b starts around a value of 10^3 near the phase transitions and goes up to 10^6 near the Kitaev point. At exactly $\phi = 3\pi/2$, the value of b is meaningless as

the parameter a is very close to zero thus killing the exponential term and leaving the constant term $c = 1$. We must make note of the point at $\phi = 1.537\pi$ which does not seem to behave like the other points. As this point is very close to the transition, we believe it to be an error, possibly due to some difficulties experienced by the DMRG algorithm in finding the ground state.

We chose not to show the values of a and c as the values appear to be very erratic and it is difficult to make sense of them. However, the values of a remain positive for all values of ϕ and are in general close to $a = 1$. For the values of c, they tend to be close to $c = 0$, however as we get close to the Kitaev point they start behaving erraticaly and sometimes become negative.

While it is unknown why these results appear so inconsistent, especially when compared to the results obtained around the antiferromagnetic point, they would certainly be improved with more computing power. Studying a larger system with more DMRG sweeps and a larger bond dimension, as well as a finer granulation of values of ϕ could provide deeper insight into the behaviour of the string order parameter on the 4-leg ladder around the antiferromagnetic point.

5.4 3-leg and 5-leg ladders

In this section, we look to extend our results for the 2-leg and 4-leg ladders to odd leg ladder systems such as a 3-leg and 5-leg ladders. As mentioned in chapter 2, when dealing with odd leg ladder systems, we have the added difficulty of the vertical boundary conditions not lining up perfectly. For this reason, unlike the even leg ladder systems, the odd leg systems are more akin to a spiral than a cylinder. Nevertheless, we can study the 3-leg and 5-leg ladders and see how the results compare to the 2-leg and 4-leg ladders.

We first set our sights on the antiferromagnetic point. As with the 2-leg and 4-leg Kitaev-Heisenberg ladders studied earlier, the method remains the same. Starting from the Kitaev-Heisenberg Hamiltonian from equation 5.1 defined on either the 3-leg or 5-leg lattice, we write the Hamiltonian as an MPO $\hat{H}$. We parametrize this Hamiltonian by setting $K = \sin\phi$ and $J = \cos\phi$, thus associating a specific Kitaev-Heisenberg Hamiltonian with each unique value of $\phi \in [0, 2\pi[$. We are once again interested in values of ϕ close to the Kitaev points at $\phi = \pi/2$ and $\phi = 3\pi/2$.

Then, starting from a random initial matrix product state $|\phi_0\rangle$, we apply the DMRG algorithm using the ITensor library to find the ground state $|\phi\rangle$ and corresponding ground state energy E associated with a specific Hamiltonian $\hat{H}(\phi)$. From this ground state, we calculate the expectation value of the string order operator as defined by equation 3.20 for each site r along the bottom two legs of the lattice. For each value of ϕ, we associate a single value O^z as defined by equation 5.2.

In the figure below, we take a look at the values of O^z as a function of ϕ close to the antiferromagnetic Kitaev point $\phi = \pi/2$ obtained for both the 3-leg and 5-leg ladders and compare these results with the results obtained for the 2-leg and 4-leg ladders. We also look at the second derivative of the ground state energy per site χ_E with respect to ϕ to identify the transition points where a second order phase transition occurs.

Given the additional interactions present most notably in the 5-leg ladder, we are limited in the size of the systems we can study. For this reason, we limit ourselves to systems of length $L = 24$. The total number of sites is given by $N = nL$ with n being the number of legs. With these system sizes, we are still able to draw conclusions from the results while keeping computation times reasonable.

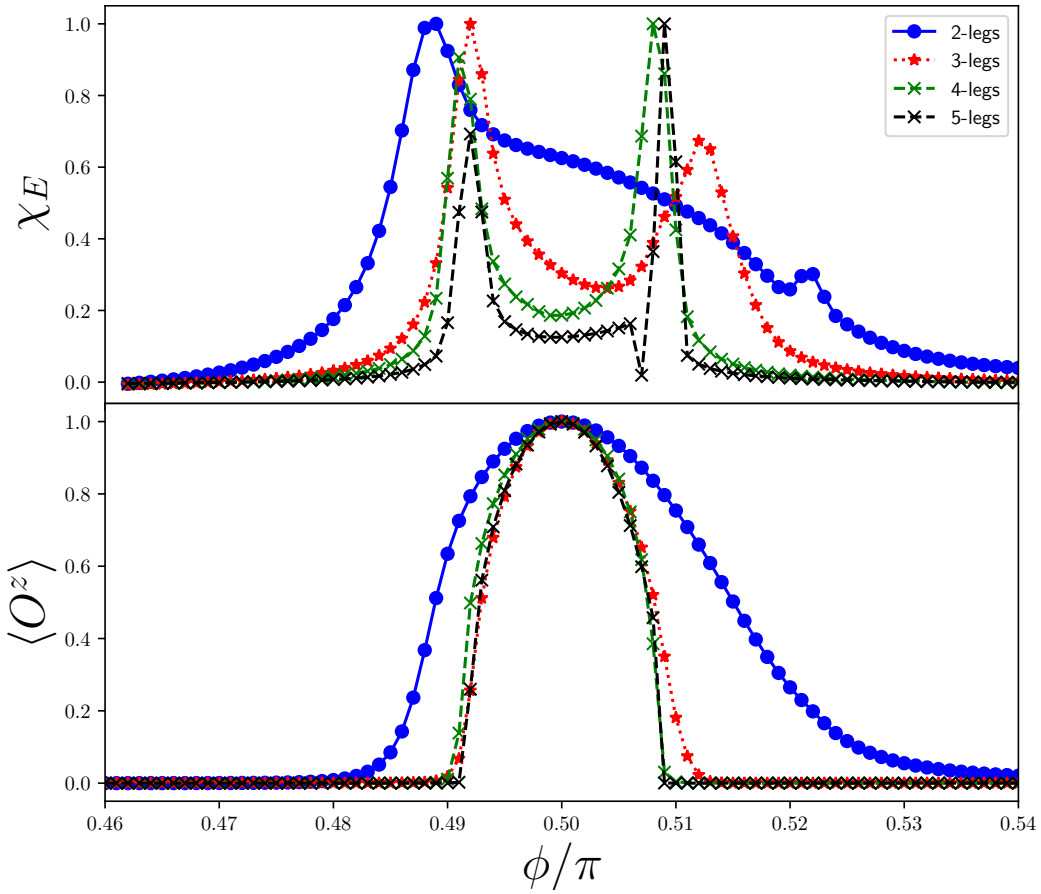

Figure 5.17: Comparison of χ_E and O^z around the antiferromagnetic point for the 2-leg, 3-leg, 4-leg and 5-leg ladders. Each ladder system is of length $L = 24$. For each system, the DMRG parameters used are $s = 15$ sweeps and a largest bond dimension of $m = 2000$. The truncation error is of the order of 10^{-9} for the 2-leg, 3-leg, and 4-leg ladders and 10^{-8} for the 5-leg ladder. The values of chi_E are normalised to allow comparison of the shape of the function between the different ladder systems.

As we can see from figure 5.17, most notably the phase transition seems to occur at very similar points for the 3-leg, 4-leg, and 5-leg ladders while the AFK phase is larger in the 2-leg ladder. Additionally, in all cases we see a good agreement between maximums of χ_E and non-zero values of O^z. Given this result, this analysis suggests that the non-local string order parameter is still present in odd leg ladder systems.

Moving on from the antiferromagnetic point, we can now have a look at the behaviour of the 3-leg and 5-leg Kitaev-Heisenberg ladders around the ferromagnetic point at $\phi = 3\pi/2$

to see if they behave differently compared to the even-leg ladder systems. The figure below shows χ_E and O^z as functions of ϕ around the ferromagnetic Kitaev point for the 2-leg, 3-leg, 4-leg, and 5-leg ladders. The values of χ_E are normalised to allow a more direct comparison of the shape of the function between the various systems.

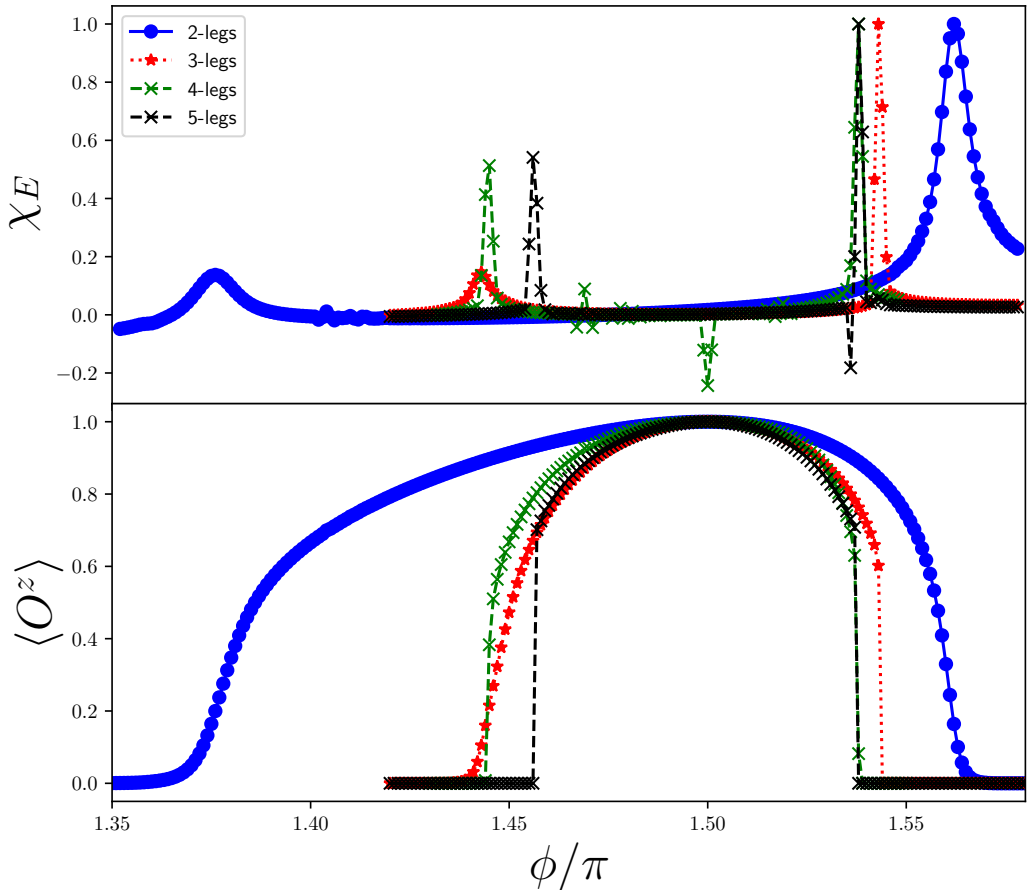

Figure 5.18: Comparison of χ_E and O^z around the ferromagnetic point for the 2-leg, 3-leg, 4-leg and 5-leg ladders.Each ladder system is of length $L = 24$. For each system, the DMRG parameters used are $s = 15$ sweeps and a largest bond dimension of $m = 2000$. The truncation error is of the order of 10^{-9} for the 2-leg, 3-leg, and 4-leg ladders and 10^{-8} for the 5-leg ladder. The values of chi_E are normalised to allow comparison of the shape of the function between the different ladder systems.

Once again we see the presence of a non-zero string order parameter inside the FK phase delimited by maximums of χ_E, thus indicating the presence of a string order parameter in odd-leg ladder systems of the Kitaev-Heisenberg model.

Let's take a closer look at the values of ϕ at which the phase transition occurs. These values are found by identifying maximums of χ_E for each system studied. Table 5.4 shows the values of ϕ at which the phase transition occurs in multileg Kitaev-Heisenberg ladders around both the antiferromagnetic and ferromagnetic points.

Table 5.1: Transition points for the AFK and FK phases in n-leg Kitaev-Heisenberg ladders

	AFK			FK		
Legs	ϕ_1	ϕ_2	$\Delta\phi$	ϕ_1	ϕ_2	$\Delta\phi$
2	0.489	0.522	0.033	1.376	1.562	0.186
3	0.492	0.512	0.020	1.443	1.543	0.100
4	0.491	0.508	0.017	1.445	1.538	0.093
5	0.492	0.509	0.017	1.456	1.538	0.082

In this table, we first label the values of ϕ at which the phase transition occurs as ϕ_1 and ϕ_2, with $\phi_1 < \phi_2$. The antiferromagnetic Kitaev phase (AFK) corresponds to the spin liquid phase around the Kitaev point at $\phi = \pi/2$ while the ferromagnetic Kitaev phase (FK) corresponds to the spin liquid phase around the Kitaev point at $\phi = 3\pi/2$. We define $\Delta\phi = \phi_2 - \phi_1$ as the width of the phase window corresponding to a Kitaev spin liquid. For all the values of ϕ in table 5.4, for the sake of simplicity we omit multiplying the results by π, for example writing $\phi = 0.5$ instead of $\phi = \pi/2$ for the antiferromagnetic Kitaev point.

From these values, we first notice that $\Delta\phi$ is smaller at the antiferromagnetic point for all legs. This is in agreement with results by Chaloupka, Jackeli, and Khaliullin [15] and Catuneanu, Sørensen, and Kee [17] who showed a smaller window for the spin liquid phase around the antiferromagnetic Kitaev point on a hexagonal cluster and a 2-leg ladder of the Kitaev-Heisenberg model respectively. However, we see that for both the AFK and the FK phases, as we increase the number of legs, the spin liquid phase around the Kitaev points gets narrower.

5.5 Pruned lattices

Returning to the 2-leg and 4-leg ladders, we mentioned in chapter 2 that we can consider the 4-leg ladder to be a system composed of two 2-leg ladders coupled by interactions labelled

z' in figure 2.6. By removing these interactions, the 4-leg ladder reduces to two independant 2-leg ladders with open boundary conditions which we referred to as the pruned 2-leg ladder. For this reason, we argued that the results obtained for the string order parameter on the 2-leg pruned ladder and the 4-leg pruned ladder should be identical. In this section, we verify this hypothesis.

Starting with the same Kitaev-Heisenberg Hamiltonian as previously used, we remove the interactions along bonds labelled z' in figures 2.4 and 2.6. We then proceed as usual by defining $K = \sin\phi$ and $J = \cos\phi$ and using DMRG to find the ground state of the Hamiltonian associated with a specific value of ϕ as a matrix product state. From this ground state, the string order parameter is calculated as a function of lattice site r using equation 3.20. We then associate a single value O^z to the string order parameter corresponding to each value of ϕ with equation 5.2. We first take a look at values close to the antiferromagnetic Kitaev point at $\phi = \pi/2$.

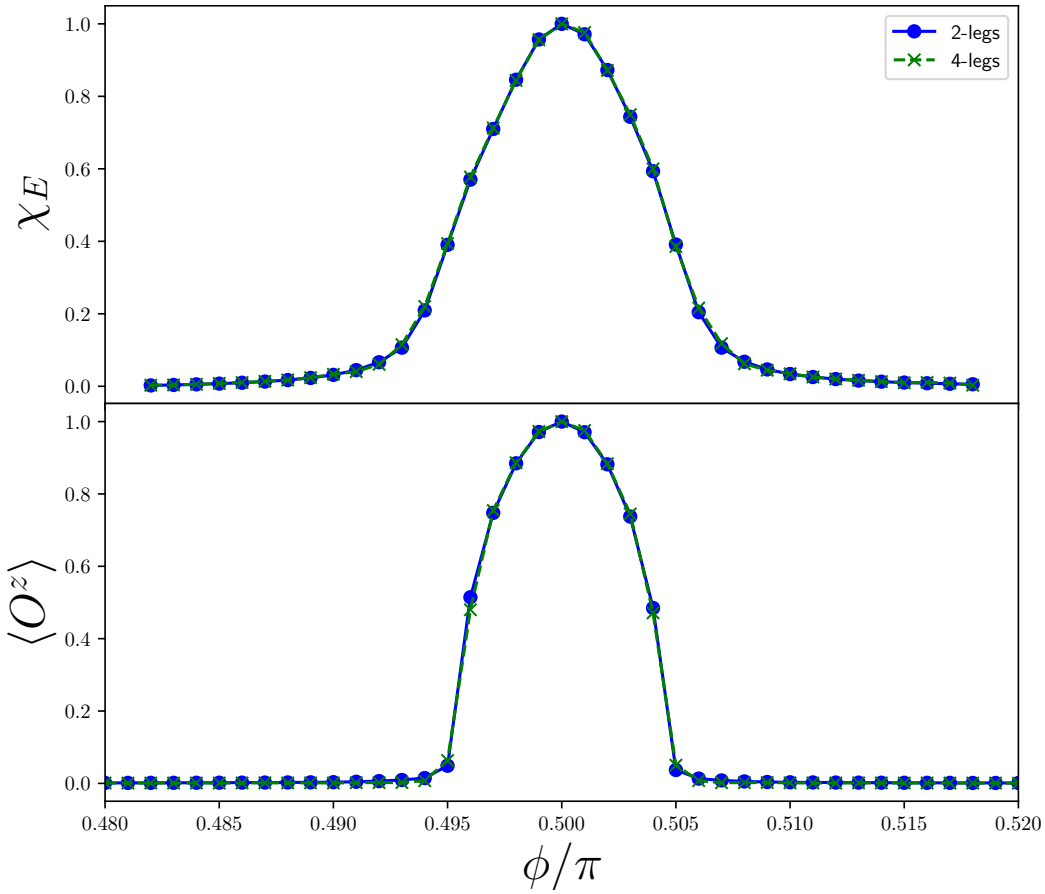

Figure 5.19: Comparison of χ_E and O^z around the antiferromagnetic point for the pruned 2-leg and 4-leg ladders. For both systems we use a length of $L = 48$ sites. The DMRG parameters used are $s = 15$ sweeps and a largest bond dimension of $m = 2000$ for both systems.

As we can see in figure 5.19, the values obtained for the 2-leg pruned and the 4-leg pruned ladders are perfectly identical. This helps confirm our hypothesis that these two lattices are equivalent and gives us confidence that our code written for the 4-leg ladder is free of errors. However, we notice significant differences between the results obtained for the pruned systems compared to the results in figure 5.3 for the unpruned systems.

First, the phase window associated with the non-zero string order parameter is much smaller in the pruned systems. In the unpruned systems, the phase boundaries are $\phi_1 = 0.489$ and $\phi_2 = 0.522$ for the 2-leg ladder and $\phi_1 = 0.491$ and $\phi_2 = 0.508$ for the 4-leg ladder. In the pruned case, we see that the string order parameter falls to zero around $\phi_1 = 0.495$ and

$\phi_2 = 0.505$, thus giving a much more narrow phase window.

Perhaps more strikingly, χ_E behaves very differently in the pruned ladders. Instead of having two distinct maximums delimiting the phase boundaries, in the pruned lattices χ_E has a single maximum exactly at the Kitaev point $\phi = \pi/2$. This could indicate that we have a higher order phase transition present. However, given the narrow nature of the phase window, it could also be due to a lack of data points and perhaps a finer granulation of the values of ϕ around the Kitaev point would reveal the second order phase transition.

Let us now focus our attention to the ferromagnetic Kitaev point at $\phi = 3\pi/2$. We proceed with the same method for finding the ground state of the Kitaev-Heisenberg model on the pruned lattices. Figure 5.20 gives the values of χ_E and O^z for the pruned lattices around the ferromagnetic Kitaev point.

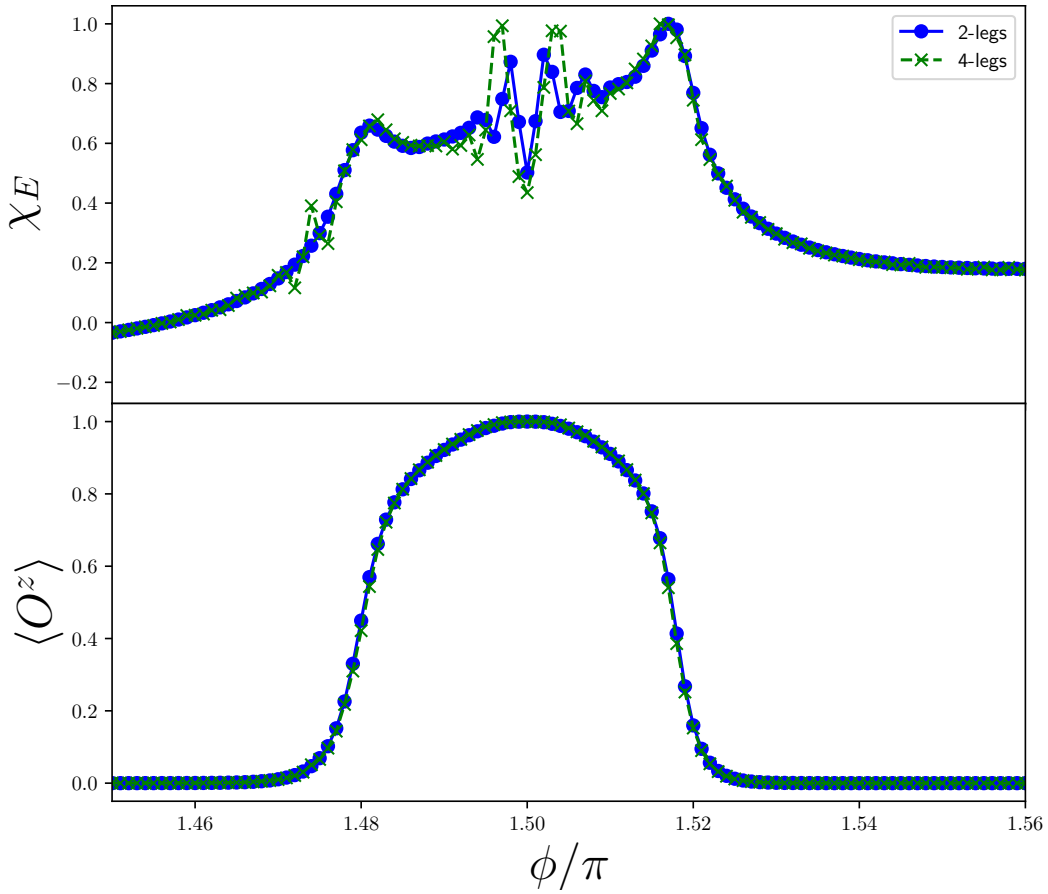

Figure 5.20: Comparison of χ_E and O^z around the ferromagnetic point for the pruned 2-leg and 4-leg ladders. For both systems we use a length of $L = 48$. The DMRG parameters used are $s = 15$ sweeps and a largest bond dimension of $m = 2000$ for both systems.

Once again we see perfect agreement between the 2-leg pruned ladder and the 4-leg pruned ladder for the values of O^z. However, while the values of chi_E generally agree, we see slight differences between the two systems. The general shape of the two functions is similar, but some scattering is present in the data obtained for the 4-leg pruned ladder. This could be attributed to small computational errors such as machine error or the DMRG algorithm getting stuck in a local minimum for the ground state energy and not quite finding the same ground state.

As was the case around the antiferromagnetic Kitaev point, we again see a narrower phase window where the string order parameter O^z is non-zero. For the pruned lattice, the phase transition occurs at $\phi_1 = 1.481$ and $\phi_2 = 1.517$ while the phase boundaries for the non-

pruned lattices are $\phi_1 = 1.376$ and $\phi_2 = 1.562$ for the 2-leg ladder and $\phi_1 = 1.445$ and $\phi_2 = 1.538$ for the 4-leg ladder.

Chapter 6

Conclusions

Throughout the course of this thesis, we set out on a search for the existence of a non-local string order parameter in multileg Kitaev-Heisenberg ladder systems. Previous results have shown that such a string order parameter exists in the 2-leg ladder and survives the Heisenberg perturbation in a certain region of the phase space close to the antiferromagnetic and ferromagnetic Kitaev points. Building upon this result, we aimed to find whether or not this non-local string order parameter survived in larger multileg ladder systems of the Kitaev-Heisenberg model. The cornerstone of this research question was to see if we could define the string order parameter in a 4-leg Kitaev-Heisenberg ladder, which is the next natural progression following the 2-leg ladder, and show that it survives the Heisenberg interaction.

Our results show that the non-local string order parameter $\langle O^z(r)\rangle$ is indeed present in the 4-leg Kitaev-Heisenberg ladder model. We find a non-zero string order parameter O^z inside the spin liquid AFK and FK phases around the Kitaev points at which the Heisenberg interaction disappears. This string order parameter is present for all system lengths studied, up to $L = 96$. Additionally, this string order parameter can be associated with a second order phase transition of the model identified by maximums of the second derivative of the ground state energy per site with respect to ϕ the system parameter.

Additionally, we were able to reproduce results obtained previously for the string order parameter on the 2-leg ladder. Comparing these results with the results on the 4-leg ladder, we see that while the string order parameter does survive the Heisenberg interaction on the 4-leg ladder, it does so in a narrower range of parameters, thus resulting in a smaller spin liquid phase around both the antiferromagnetic and ferromagnetic Kitaev points.

However, a closer look at the behaviour of the string order parameter as a function of lattice site r reveals differences between the 4-leg ladder and the 2-leg ladder. In the 2-leg case, as we move along the lattice and r increases, for values of ϕ inside the spin liquid phases the string order parameter $\langle O^z(r)\rangle$ goes to a constant value. Conversely, in the 4-leg case, $\langle O^z(r)\rangle$ does not go to a constant value as r increases and instead goes to zero even inside the spin liquid phases when a Heisenberg interaction is present. This could indicate that for large systems, the string order parameter only exists at short range and decays as we move along the lattice before eventually disappearing.

To answer this question fully, we would need to study systems of length L larger than what we were able to do in the context of this thesis. The DMRG algorithm used becomes very time consuming and memory intensive for large systems with many interactions. This means that we were limited to a system length of at most $L = 96$ for the 4-leg ladder. Even then, the DMRG parameters used had to be reduced thus making the results obtained less precise and it still took up to 7 days to obtain the final results. This made it impractical to do multiple attempts at improving the algorithm. As such, it became more reasonable to study a system length of $L = 48$ for the 4-leg ladder. While this allows for more manageable computing times, our algorithm seems to struggle in obtaining consistent results for certain values of the ferromagnetic Kitaev phase, as can be seen in figure 5.2. When making exponential fits to $\langle O^z(r)\rangle$ on the 4-leg ladder, the relatively low number of points available for the fit due to the limit of the system size coupled with inconsistent results sometimes results in a poor fit. This leads to inconclusive results for the exponential fit of the string order parameter in the ferromagnetic Kitaev phase of the 4-leg ladder.

To remedy this problem, a deeper dive into the workings of the DMRG algorithm could prove valuable. At the moment, it is unknown why the DMRG algorithm seems to struggle with finding consistent values of the ground state energy for certain values of the FK phase. This could be due to difficulties in differentiating low lying excited states from the ground state, or perhaps an unknown phenomenon could be at play. Alternatively, a different method for finding the ground state in large 4-leg ladder systems could prove more effective.

Certain optimizations of the code used could also prove beneficial and allow for the study of larger systems even with the same computational resources available. For example, instead of using a random initial state, we could make a more educated guess for a starting point before applying the DMRG algorithm. This could allow a faster convergence towards the ground state and improve computing times. If we are able to study larger systems with-

out compromising precision and obtain reliable data, we would be able to obtain more data points for the string order parameter at each lattice site, thus improving the quality of the exponential fits and perhaps allowing for more conclusive data, notably in the 4-leg ladder.

Moving on to the odd-leg ladders, we showed that the non-local string order parameter $\langle O^z(r)\rangle$ is present in the 3 and 5-leg ladders. We notice a trend where while the SOP is present and survives a Heisenberg interaction, the spin liquid phase gets narrower around both the antiferromagnetic and the ferromagnetic Kitaev points when adding more legs to the system. In further studies, it would be interesting to study a 6-leg and 7-leg ladder to see if this pattern holds and try to predict if the spin liquid phases are still present in a full 2D system or if they eventually disappear. Additionally, we could take a look at the string order parameter as a function of lattice site r in much the same way as we did with the 2-leg and 4-leg ladders to see if the SOP eventually becomes constant or if it goes to zero as r gets large.

While our definition of the odd-leg ladders with the slanted vertical boundary conditions did give us results that seem to align with results obtained for the even-leg ladders, it is possible that a better definition exists. For example, we kept a rectangular shape to the overall lattice. One modification could be to omit sites in the top left and bottom right corners and instead have a lattice with a parallelogram shape. Such a lattice has been defined for a 3-leg ladder by Khait, Stavropoulosm, Kee, and Kim [23] for the study of spin-one Kitaev quantum spin liquids. Such a lattice, which could be extended to the 5-leg ladder, could represent a more natural cutout of a 2 dimensional honeycomb lattice.

Lastly, the results obtained on the pruned ladder show that when we set $z' = 0$, the 2-leg pruned ladder and 4-leg pruned ladder become identical as far as ground state energy and values of the string order parameter are concerned. However, the AFK and FK phases associated with the string order parameter become much more narrow on the pruned lattice. Thus, these z' interactions could prove vital for the existence of the SOP. Additionally, in the AFK phase, χ_E does not seem to display a second order phase transition and more research could go into explaining why that is.

Overall, we were able to show the existence of a non-local string order parameter in the 4-leg Kitaev-Heisenberg ladder. This string order parameter is present around both the antiferromagnetic and the ferromagnetic points. However, the range of parameters in which the SOP survives the Heisenberg interaction is narrower in the 4-leg ladder compared to the 2-leg ladder. Additionally, the SOP seems to decay at long range on the 4-leg ladder even inside

the spin liquid phases.

To obtain more conclusive results, it would be beneficial to study larger systems by improving the numerical techniques used and making use of additional computational resources. To obtain more precise values of the phase boundaries, a finer granulation of the values of ϕ in the phase diagram could give more insight into the behaviour of the system close to the phase transitions. In order to determine definitively if the SOP survives the Heisenberg interaction in a real Kitaev material, systems of n legs with n being larger than 4 could be studied to see if the spin liquid phase eventually remains at a constant width even with additional legs or if this spin liquid phase eventually disappears. Another possible interest is to study the pruned systems with values of the z' interactions other than 0 or 1. This could give greater insight into the importance of the z' interactions for the realisation of a quantum spin liquid.

Bibliography

[1] Lucile Savary, Leon Balents. Quantum Spin Liquids. *arXiv preprint*, 1601.03742, 2016.

[2] Entanglement. Meriam-Webster Dictionary. 2022 `https://www.merriam-webster.com/dictionary/entanglement`.

[3] Richard Jozsa, Noah Linden. On the role of entanglement in quantum-computational speed-up. *Proc. R. Soc. Lond.*, A.45920112032, 2003.

[4] Peter W. Shor. Algorithms for quantum computation: discrete logarithms and factoring. *Proceedings 35th Annual Symposium on Foundations of Computer Science*, pp. 124-134, 1994.

[5] Abdullah Ash Saki, Mahabubul Alam, Swaroop Ghosh. Study of Decoherence in Quantum Computers: A Circuit-Design Perspective. *arXiv preprint*, 1904.04323, 2019.

[6] A.Yu. Kitaev. Fault-tolerant quantum computation by anyons. *Annals of Physics*, Volume 303, Issue 1, Pages 2-30, 2003.

[7] F. Wilczek. Fractional Statistics and Anyon Superconductivity. *World Scientific*, Singapore, 1990.

[8] Chetan Nayak, Steven H. Simon, Ady Stern, Michael Freedman, Sankar Das Sarma. Non-Abelian Anyons and Topological Quantum Computation. *Reviews of Modern Phisics*, 80, 2007.

[9] Alexei Kitaev. Anyons in an exactly solved model. *Annals of Physics*, 321 2, 2006.

[10] Leon Balents. Spin liquids in frustrated magnets. *Nature*, 464 199-208, 2010.

[11] George Jackeli, Giniya Khaliullin. Mott Insulators in the Strong Spin-Orbit Coupling Limit: From Heisenberg to a Quantum Compass and Kitaev Models. *Phys. Rev. Lett.*, 102, 017205, 2009.

[12] K. W. Plumb, J. P. Clancy, L. Sandilands, V. Vijay Shankar, Y. F. Hu, K. S. Burch, Hae-Young Kee, Young-June Kim. $\alpha - \mathrm{RuCl_3}$: A spin-orbit assisted Mott insulator on a honeycomb lattice. *Phys. Rev. B*, 90, 041112, 2014.

[13] Jiri Chaloupka, George Jackeli, Giniyat Khaliullin. Kitaev-Heisenberg Model on a Honeycomb Lattice: Possible Exotic Phases in Iridium Oxides $A_2\mathrm{IrO_3}$. *Phys. Rev. Lett.*, 105, 027204, 2010.

[14] Jeffrey G. Rau, Eric Kin-Ho Lee, Hae-Young Kee. Generic Spin Model for the Honeycomb Iridates beyond the Kitaev Limit. *Phys. Rev. Lett.*, 112, 077204, 2014.

[15] Jiri Chaloupka, George Jackeli, Giniyat Khaliullin. Zigzag Magnetic Order in the Iridium Oxide $\mathrm{Na_2IrO_3}$. *Phys. Rev. Lett.*, 110, 097204, 2013.

[16] Xiao-Yong Feng, Guang-Ming Zhang, Tao Xiang. Topological Characterization of Quantum Phase Transitions in a Spin-1/2 Model. *Phys. Rev. Lett.*, 98, 087204, 2007.

[17] Andrei Catuneanu, Erik S. Sørensen, Hae-Young Kee. Non-local String Order Parameter in the $S = 1/2$ Kitaev-Heisenberg Ladder. *Phys. Rev. B*, 99, 195112, 2019.

[18] Andrei Catuneanu, Erik S. Sørensen, Hae-Young Kee. Supplementary Material for "Non-local String Order Parameter in the $S = 1/2$ Kitaev-Heisenberg Ladder". *Phys. Rev. B*, 99, 195112, 2019.

[19] Steven R. White. Density Matrix Formulation for Quantum Renormalization Groups. *Phys. Rev. Lett.*, 69, 19, 2863–2866, 1992.

[20] U. Schollwock. The Density-Matrix Renormalization Group. *Rev. Mod. Phys.* 77, 259, 2005.

[21] U. Schollwock. The Density-Matrix Renormalization Group in the Age of Matrix Product States. Annals of Physics 326, 1, 2011.

[22] Matthew Fishman, Steven R. White, E. Miles Stoudenmire. The ITensor Software Library for Tensor Network Calculations. *arXiv preprint*, 2007.14822, 2021.

[23] Ilia Khait, Peter P. Stavropoulos, Hae-Young Kee, Yong Baek Kim. Characterizing spin-one Kitaev quantum spin liquids. *Phys. Rev. Research*, 3, 013160, 2021.